Published in final edited form as:
Exp Eye Res. 2014 March ; 120: 138–151. doi:10.1016/j.exer.2014.01.018.

Lipid-Protein Interactions in Plasma Membranes of Fiber Cells Isolated from the Human Eye Lens

Marija Raguz[a,c], **Laxman Mainali**[a], **William J. O'Brien**[b], and **Witold K. Subczynski**[a,*]

[a]Department of Biophysics, Medical College of Wisconsin, Milwaukee, WI 53226, USA

[b]Department of Ophthalmology, Medical College of Wisconsin, Milwaukee, WI 53226, USA

[c]Department of Medical Physics and Biophysics, School of Medicine, University of Split, Split, Croatia

Abstract

The protein content in human lens membranes is extremely high, increases with age, and is higher in the nucleus as compared with the cortex, which should strongly affect the organization and properties of the lipid bilayer portion of intact membranes. To assess these effects, the intact cortical and nuclear fiber cell plasma membranes isolated from human lenses from 41- to 60-year-old donors were studied using electron paramagnetic resonance spin-labeling methods. Results were compared with those obtained for lens lipid membranes prepared from total lipid extracts from human eyes of the same age group [Mainali,L., Raguz, M., O'Brien, W. J., and Subczynski, W. K. (2013) Biochim. Biophys. Acta]. Differences were considered to be mainly due to the effect of membrane proteins. The lipid-bilayer portions of intact membranes were significantly less fluid than lipid bilayers of lens lipid membranes, prepared without proteins. The intact membranes were found to contain three distinct lipid environments termed the *bulk lipid domain*, *boundary lipid domain*, and *trapped lipid domain*. However, the *cholesterol bilayer domain*, which was detected in cortical and nuclear lens lipid membranes, was not detected in intact membranes. The relative amounts of bulk and trapped lipids were evaluated. The amount of lipids in domains uniquely formed due to the presence of membrane proteins was greater in nuclear membranes than in cortical membranes. Thus, it is evident that the rigidity of nuclear membranes is greater than that of cortical membranes. Also the permeability coefficients for oxygen measured in domains of nuclear membranes were significantly lower than appropriate coefficients measured in cortical membranes. Relationships between the organization of lipids into lipid domains in fiber cells plasma membranes and the organization of membrane proteins are discussed.

Keywords

cholesterol; membrane domains; fluidity; hydrophobic barrier; oxygen permeation; spin labeling

[*]**Corresponding Author**: Witold K. Subczynski, Department of Biophysics, Medical College of Wisconsin, 8701 Watertown Plank Road, Milwaukee, WI 53226, USA. Tel: (414) 456-4038; Fax: (414) 456-6512; subczyn@mcw.edu.

1. Introduction

The human eye lens is an avascular organ which is built from thousands of concentric layers of fiber cells (Beebe, 2003). Lens fiber cells lose their intracellular organelles soon after they are formed (Bassnett et al., 2011; Rafferty, 1985; Wride, 2011), and the plasma membrane becomes essentially the only membranous structure of matured fiber cells which accounts for mostly all lens lipids. Membrane proteins allow communication between tightly packed layers of fiber cells and active transport of water, ions, and other small molecules (Dahm et al., 2011; White and Bruzzone, 2000). The lipid bilayer portion of the membrane determines bulk membrane properties (including diffusion barriers) (Borchman and Yappert, 2010; Subczynski et al., 2012) and also can affect the properties of membrane proteins (Epand, 2005; Reichow and Gonen, 2009; Tong et al., 2012; Tong et al., 2013).

The four major factors that can significantly affect the organization and properties of the lipid bilayer portion of the fiber-cell membranes of human lenses are: (1) unusually high level of saturation (Deeley et al., 2008; Li et al., 1985; Yappert et al., 2003), (2) abundance of sphingolipids, mainly dihydrosphingomyelin (Borchman et al., 1994; Deeley et al., 2008; Yappert and Borchman, 2004; Yappert et al., 2003), (3) extremely high cholesterol (Chol) content (Li et al., 1985, 1987; Rujoi et al., 2003; Zelenka, 1984), and (4) high density of membrane proteins (Bassnett et al., 2011; Gonen et al., 2004; Kistler and Bullivant, 1980; Li et al., 1986; Li et al., 1985). The former three factors were investigated and discussed in many papers and results are summarized in two recent reviews (Borchman and Yappert, 2010; Subczynski et al., 2012). The latter factor is less investigated. Recently, we published data where we compared properties of lens lipid membranes—i.e., membranes without a protein component—with those of the lipid bilayer portion of intact membranes isolated from eyes of the two-year-old porcine (Mainali et al., 2012a). In this manuscript we compare the organization and properties of lens lipid membranes and intact membranes isolated from the cortex and nucleus of the human eye lens from 41- to 60-year-old human donors. In addition, we were able to evaluate the relative amounts of lipids in membrane domains formed due to the presence of membrane proteins. This age group contains already matured lens fiber cells with well-separated cortical and nuclear regions. Thus, this work should form good starting points for further research on lenses from different age groups and on cataractous lenses.

In earlier works (Mainali et al., 2011b; Mainali et al., 2013c; Raguz et al., 2008, 2009; Widomska et al., 2007a) we showed that properties of membranes derived from the total lipids extracted from animal lens cortex and nucleus are mostly determined by the saturating Chol content. The effect of the phospholipid (PL) composition (which for eye lenses drastically changes between species, with age, and with location in the lens (Estrada et al., 2010; Huang et al., 2005; Hughes et al., 2012; Li and So, 1987; Li et al., 1987; Mainali et al., 2012a, 2013c; Paterson et al., 1997; Raguz et al., 2009; Rujoi et al., 2004; Truscott, 2000; Yappert and Borchman, 2004; Yappert et al., 2003)) on these properties in membranes saturated with Chol was minor. Those studies were summarized in the review (Subczynski et al., 2012). In a recent paper (Mainali et al., 2012a), we showed that the organization and properties of the lipid bilayer portion of intact fiber cell plasma membranes isolated from cortex and nucleus of porcine eye lenses is strongly affected by the protein content in membranes. Nuclear membranes, because of the higher protein content (Li et al., 1986; Li et al., 1985), were more strongly affected.

The organization of the lipid bilayer portion of the fiber cell membrane is capable of functionally altering the physiological properties of the cell. This is especially true for fiber cells in which the plasma membrane together with the cytoskeleton is primarily the only cellular supramolecular structure (Bassnett and Beebe, 1992; Dahm, 1999). It seems that the

major function of membrane proteins in the eye lens is related to the communication between tightly packed layers of fiber cells. The lipid bilayer portion of the membrane, in which these proteins are immersed, would be expected to influence this function. This is achieved in fiber cell membranes by formation of the boundary and trapped lipid domains with high diffusion barriers for transport of both polar and hydrophobic small molecules. High hydrophobicity of the interiors of these domains ensures that that "leaking" of water, ions, and other small polar and ionic molecules across these domains is minimized, and their transport is tightly controlled by membrane proteins. High rigidity of these domains, which reaches almost the rigid limit in the membrane center, ensures high barrier for transport of small hydrophobic molecules across the plasma membrane and minimal uncontrolled "leaking" of these molecules.

In the studies reported here we focused on lipid-protein interactions in plasma membranes of fiber cells isolated from human eye lenses. These studies are a natural continuation of the recently published work on properties of membranes derived from the total lipids extracted from human lenses (Mainali et al., 2013c). Four lipid domains were hypothesized to exist in fiber cell membranes of the human eye lens, namely, the bulk lipid domain, boundary lipid domain, trapped lipid domain, and cholesterol bilayer domain (CBD)[1]. We used electron paramagnetic resonance (EPR) spectroscopy with stearic acid and Chol analog spin labels (Fig. 1). Conventional (Griffith and Jost, 1976; Kawasaki et al., 2001; Marsh, 2008, 2010) and saturation recovery (SR) (Ashikawa et al., 1994a; Kawasaki et al., 2001; Subczynski et al., 1998) EPR spin-labeling approaches were used to discriminate different membrane domains created in the lipid bilayer by the presence of membrane proteins, but also to assess membrane properties as a function of depth in domains (Subczynski et al., 2010; Subczynski et al., 2009).

2. Materials and Methods

2.1. Materials

Doxylstearic acid spin labels (*n*-SASL, *n* = 5, 7, 9, 12, or 16) and androstane spin label (ASL) (see Fig. 1 for their structure) were purchased from Molecular Probes (Eugene, OR). Other chemicals of at least reagent grade were purchased from Sigma-Aldrich (St. Louis, MO).

2.2. Isolation of intact membranes from cortical and nuclear fiber cell membranes

Fifty clear human lenses from donors ranged in age from 41 to 60 years were obtained from the Lions Eye Bank of Wisconsin. The cortical and nuclear regions of these lenses were separated based on differences in tissue consistency (Estrada and Yappert, 2004; Rujoi et al., 2003). Cortical and nuclear intact membranes were isolated from portions (about twenty lenses) of the cortical and nuclear tissue based on minor modifications of the method developed by Bloemendal et al.(Bloemendal et al., 1972)], as reported earlier (Cenedella and Fleschner, 1992; Chandrasekher and Cenedella, 1995; Lim et al., 2005)]. The cortical and

[1]The bulk lipid domain in the intact membrane is formed by the lipid bilayer which is not affected by the presence of integral membrane proteins, with the same (or almost the same) properties as a lipid bilayer membrane formed from the total lipid extract from the intact membrane. The boundary lipid domain around integral proteins is formed by protein-bound, immobilized phospholipids (a single lipid layer coating the hydrophobic surface of the protein, regardless of the amount of fluid bulk lipids) (Jost et al., 1973). However, the exchange rate between boundary and bulk lipids is of the order of magnitude of 10^7 s^{-1} or greater (East et al., 1985; Marsh, 1997; Ryba et al., 1987). The trapped lipid domain, called also the slow oxygen transport (SLOT) domain, is formed by lipids in contact with two proteins and/or by lipids in contact with proteins and boundary lipids (Ashikawa et al., 1994b). The exchange rate of lipids between this domain and bulk plus protein-boundary regions is of the order of magnitude of 10^5 s^{-1} or smaller (Kawasaki et al., 2001). The cholesterol bilayer domain (CBD) is a pure cholesterol bilayer immersed in the bulk phospholipid-cholesterol membrane (phospholipid bilayer saturated with cholesterol, which is in the liquid-ordered phase) (Mason et al., 2003; Raguz et al., 2011a, b).

nuclear tissues were homogenized separately, each in 25 mL of *buffer A* (5 mM Tris HCL, 5 mM EDTA, 5 mM EGTA, pH 8.0). The homogenate was centrifuged (29000 g, 20 min, 4°C). The pellet was washed five times with *buffer B* (5 mM Tris HCL, 2 mM EDTA, 2 mM EGTA, pH 8.0) and recovered by centrifugation (29000 g, 20 min, 4°C). Each time special care was taken to produce a uniform suspension by repeatedly aspirating the solution through a syringe fitted with an 18-gauge needle. Finally, the pellet was washed and resuspended with *buffer C* (0.1 M borate, pH 9.5) and stored at −20°C.

We also made three separate isolations of cortical and nuclear intact membranes from three pairs of lenses from three different donors. Because of the limited amount of samples we were able to use only one spin label (we chose 12-SASL) for each preparation. Results from these measurements are presented as mean values with standard deviations and are included in appropriate figure captions and tables.

2.3. Isolation of total lipids from cortical and nuclear fiber cell membranes for analysis of lipid composition

The total lipids from portions (about thirty lenses) of the cortical or nuclear samples were extracted separately based on minor modifications of the Folch procedure (Folch et al., 1957). The tissue samples were gently mashed in a 500 mL Erlenmeyer flask with the pestle from a tissue homogenizer to which ca. 200 mL of methanol/chloroform (2:1 v:v) mixture was added, and the slurry was stirred for 30 minutes. The sample was distributed to corex centrifuge tubes and centrifuged at 5000 rpm for 30 minutes. The supernatants were poured into a separatory funnel, and water and methanol were added so that the final ratio of methanol/chloroform/water was 2:1:1 (v/v). The chloroform layer was removed and the water layer was extracted two more times with chloroform. The chloroform layers were pooled, dried with $MgSO_4$, filtered, and the solvent was removed. The resultant lipid samples were used for measurements of properties of lens lipid membranes, which provided control data for the present studies (Mainali et al., 2013c). Samples from these extractions were sent to Avanti Polar Lipids (Alabaster, AL) for analysis. The relative retios of lipids for the cortex and nucleus samples, respectively, were as follows: 1.38 and 2.1 for Chol/PL, 0.22 and 0.21 for PC/PL, 0.59 and 0.61 for SM/PL, 0.08 and 0.06 for PS/PL, and 0.10 and 0.11 for PE/PL. The relative abundance of PL classes (PC, phosphatidylcholine; SM, sphingomyelin plus dihydrosphingomyelin; PS, phosphatidylserine; PE, phosphatidylethanolamine) is close to the amount reported in (Deeley et al., 2008).

2.4. Preparation of samples for EPR measurements

In studies of intact membranes we use *n*-SASLs and ASL (Fig. 1) that allows us to locate the nitroxide moiety of a spin label at different depths and in different domains in the lipid bilayer portion of intact fiber cell plasma membranes. Spin-labeling was performed as described earlier (Ligeza et al., 1998; Mainali et al., 2012a). The film of *n*-SASL was prepared on the bottom of a test tube by drying the appropriate amount of spin label in chloroform (usually ~20 μL of 1 mM solution). Only one type of *n*-SASL was present in each sample. Intact membrane suspensions (~0.2 mL) were added to the test tubes and shaken for about two hours at room temperature. Control measurements demonstrated that this incubation time was sufficient to incorporate nearly all of the spin-label molecules into the membranes. To ensure that the maximum amount of supernatant was removed, membrane suspensions were centrifuged twice using Eppendorf centrifuge (12000g, 20 min, 4°C), and the loose pellet was transferred to a 0.6 mm i.d. capillary made of gas-permeable methylpentene polymer (TPX) and used for EPR measurements (Subczynski et al., 2005).

2.5. EPR measurements

To further increase the signal-to-noise ratio, samples in TPX capillaries were centrifuged as described in (Subczynski et al., 2005). Conventional EPR spectra were recorded with a Bruker EMX spectrometer equipped with temperature-control accessories. All spectra were obtained at 37°C with a modulation amplitude of 1.0 G and an incident microwave power of 5.0 mW. To assess fluidity, maximum splitting values were measured for each component directly from the EPR spectra as indicated in Fig. 2A and B (Mainali et al., 2013c)). Samples were thoroughly deoxygenated, yielding correct EPR line shapes. Maximum splitting values were measured within the precision of ±0.25 G for lens lipid membranes and within the precision of ±0.5 G and ±1.0 G for fluid and immobilized components, respectively, in intact membranes. To measure hydrophobicity, the *z*-component of the hyperfine interaction tensor of the *n*-SASL, A_Z, was determined from the EPR spectra for samples frozen at −165°C and recorded with a modulation amplitude of 2.0 G and an incident microwave power of 2.0 mW (see (Subczynski et al., 1994)). Values of $2A_Z$ were measured within the precision of ±1.0 G.

Spin-lattice relaxation times, T_1s, of spin labels were determined by analyzing the SR signal of the central line obtained by short-pulse SR EPR at X-band for deoxygenated samples (Kawasaki et al., 2001; Subczynski et al., 1989; Yin and Subczynski, 1996). Accumulations of the decay signals were carried out with 2048 data points on each decay. For measurements of the oxygen transport parameter (OTP), the sample was equilibrated with the same gas that was used for temperature control (*i.e.*, a controlled mixture of nitrogen and dry air adjusted with flowmeters [Matheson Gas Products, model 7631H-604]) (Kusumi et al., 1982; Subczynski et al., 1992) and SR signals were recorded. SR signals were fitted by single- or double-exponential functions. The uncertainties in the measurements of decay time from the fits were usually less than 0.05%, whereas the decay times determined from sample to sample were within a precision of ±3% when a single-exponential fit was satisfactory and within a precision ±5% and ±10% for longer and shorter recovery time constants when a double-exponential fit was satisfactory.

2.6. Calculation of the membrane permeability coefficient for oxygen

Knowledge of the profiles of the OTP makes it possible to calculate a significant membrane characteristic—namely, the permeability coefficient for oxygen across the membrane. This method is based on the work of Subczynski et al. (Subczynski et al., 1989), and calculations for this method are explained in detail in our earlier papers (Subczynski et al., 1991; Widomska et al., 2007a). In the presented research the profiles of the OTP were obtained with *n*-SASL only across the hydrocarbon region of the lipid bilayer portion of the intact membranes and calculated values of the membrane permeability coefficient for oxygen characterize permeability properties of this membrane portion. The precision of this evaluation is ±30% (see sect. 3.1 in (Widomska et al., 2007b)).

3. Results

3.1. Parameters obtained from EPR spectra and SR signals

Figure 2A and B shows representative conventional EPR spectra for 5- and 12-SASL in cortical intact membranes. Because of the overlapping of spectra coming from *n*-SASLs in different membrane domains, we used the maximum splitting as a convenient spectral parameter which reports membrane fluidity at a certain depth in the membrane. This additionally allows discrimination of membrane domains as indicated in spectrum of 12-SASL which clearly shows one weakly immobilized component (2) and one strongly immobilized component (1). A very small amount of *n*-SASL remains free in the surrounding buffer (component 3 in Fig. 2A and B). This component does not interfere with

measurements of maximum splitting of spectra coming from spin labels in the lipid environment of intact membranes (components 1 and 2 in Figs. 2A and B).

For fast anisotropic motion the maximum splitting is directly related to the order parameter (Hubbell and McConnell, 1968) that indicates the amplitude of the wobbling motion of the appropriate segment of the alkyl chain of *n*-SASL (Kusumi et al., 1986). These conditions are fulfilled for the spectral component with smaller values of the maximum splitting. The maximum splitting values of the second component are much larger and are close to those for rigid limit conditions. At these conditions, the maximum splitting includes contribution of both the order and rotational mobility of the appropriate segment of the alkyl chain of *n*-SASL (Budil et al., 1996; Schreier et al., 1978).

Another, more straightforward way of displaying membrane fluidity is through profiles of the spin-lattice relaxation rate (T_1^{-1}) obtained from SR EPR measurements of *n*-SASLs in deoxygenated samples. The spin-lattice relaxation rate depends primarily on the rotational motion of the nitroxide moiety within the lipid bilayer (Mailer et al., 2005; Robinson et al., 1994), hence, T_1^{-1} can be used as a convenient quantitative measure of membrane fluidity (Mainali et al., 2011a; Mainali et al., 2013a). The fluidity in this display reflects rate of motions of the nitroxide moiety rigidly attached to the Cn carbon atom of the alkyl chain, and thus, the rate of motions of this fragment of the alkyl chain.

Representative SR signals are shown in Fig. 3 for cortical intact membranes for phospholipid and cholesterol analog spin labels. As can be seen, the SR signal of 7-SASL (Fig. 3A) is successfully fit only with double exponential functions, both in the absence and presence of oxygen. This indicates that this spin label is located in two environments with different fluidities and different OTPs. SR signals from other *n*-SASLs applied for intact cortical and nuclear membranes can be fitted satisfactory only with two exponentials in both the presence of oxygen and in its absence (signals not shown). Thus, two lipid environments are detected, with different fluidities and different OTPs at all depths in the lipid bilayer portion of the intact membranes.

The above approaches describe membrane organization and fluidity reporting directly on the motion and order of PL alkyl chains. Membrane fluidity can also be reported on the motion of molecular oxygen within the membrane. In this method the observed parameter is the spin-lattice relaxation time of lipid spin labels (measured as shown in Fig. 3), and the measured value is the bimolecular collision rate between molecular oxygen and the nitroxide moiety of spin labels (Subczynski et al., 2007). The method is extremely sensitive to changes in the local oxygen diffusion-concentration product (around the nitroxide moiety), which is expressed as the OTP (Kusumi et al., 1982). To obtain profiles of the OTP, spin lattice relaxation times for *n*-SASLs have to be measured for deoxygenated samples and for samples equilibrated with air at indicated temperature (see detailed description in (Subczynski et al., 2007)).

SR signals from ASL in the absence and presence of oxygen in cortical (Fig. 3B) and nuclear membranes (data not shown) were satisfactory fitted only to double exponential curves. Therefore, ASL, similarly to *n*-SASLs, can also discriminate two lipid environments with different fluidity and different values of the OTP.

Figure 2 contains also representative EPR spectra of 5-SASL (C) and 12-SASL (D) in a frozen solution of cortical intact membranes and shows the method of measuring $2A_Z$ values. Smaller $2A_Z$ values indicate higher hydrophobicity. Thus, smaller $2A_Z$ value from the spectrum of 12-SASL compared with that of 5-SASL indicates that the membrane interior is more hydrophobic than the region close to the membrane surface. In the profiles

of membrane hydrophobicity (see Sect. 3.5), $2A_Z$ values are plotted as a function of the position of the nitroxide moiety of the spin label within the lipid bilayer. For brevity, we relate the local hydrophobicity as observed by $2A_Z$ to the hydrophobicity (or ε) of the bulk organic solvent by referring to Fig. 2 in (Subczynski et al., 1994).

ASL is a spin-labeled cholesterol analog (Fig. 1) that should determine the distribution and properties of cholesterol in intact membranes. ASL, when incorporated into cortical intact membranes yields one-component EPR spectrum (component 2 in Fig. 2G) and when incorporated into nuclear membranes, two-component spectrum (components 1 and 2 in Fig. 2H). The spectrum from cortical intact membranes is practically identical to spectra from cortical and nuclear lens lipid membranes indicating that ASL cannot discriminate any lipid domain formed by the presence of integral proteins (showing only component 2). However, when the amount of proteins increases in nuclear intact membranes, the strongly immobilized component in the EPR spectrum is clearly present (component 1 in Fig. 2H). Similarly, in porcine intact membranes (Mainali et al., 2012a), ASL gives one-component EPR spectrum in cortical membranes (identical to induces formation of boundary lipids, which ASL cannot discriminate (but see Discussion). those in the cortical porcine lens lipid membrane) and twocomponent spectrum in nuclear membranes (one similar to those in the nuclear porcine lens lipid membrane and one coming from very rigid environment). We hypothesize that in nuclear intact membranes the immobilized component is formed by ASL molecules trapped within aggregates of proteins that saturate the membrane. In cortical membranes, the amount of membrane proteins is significantly smaller and, thus, mainly

3.2. Order and fluidity of phospholipid alkyl chains

3.2.1. Conventional EPR—Figure 4A and B shows profiles of the maximum splitting values obtained, as indicated in Fig. 2A and B, from *n*-SASL located at different depths in different membrane domains in cortical and nuclear intact membranes. Larger values indicate smaller fluidity and greater order of alkyl chains. EPR spectra of 12- and 16-SASL clearly show one weakly and one strongly immobilized component. However, the outermost peaks in the EPR spectra of 5-, 7-, and 9-SASL in both cortical and nuclear intact membranes cannot discriminate these components because their positions are very close to each other and only maximum splitting of the strongly immobilized component can be measured. In each membrane, profiles across two domains are presented: one across a more fluid domain and the other across a very rigid domain. Comparison of these profiles with those obtained across cortical and nuclear lens lipid membranes (Fig. 4C and D) indicates that profiles across more fluid domains are very similar to those of lens lipid membranes. We assigned this domain as a bulk lipid domain, which appears to be not affected by the presence of membrane proteins. This domain can be discriminated using conventional EPR spectra only with 12- and 16-SASL. The remaining profile of strongly immobilized lipids, formed as a result of the interaction of lipids with membrane proteins, was assigned to the boundary plus trapped lipid domain (see also Sect. 3.1 in (Mainali et al., 2012a)). Maximum splitting values in EPR spectra from membranes reconstituted with monomers or aggregates of integral membrane proteins containing boundary lipids and/or trapped lipids (Ashikawa et al., 1994a; Kawasaki et al., 2001; Marsh et al., 1982) are similar to those from intact membranes.

Maximum splitting values measured for 12- and 16-SASL in the most immobilized lipid domain are close to the rigid limit values for these spin labels (compare values in Fig. 4 with those in Fig. 7, remembering that the rigid limit value is the $2A_Z$ value). Thus, the alkyl chains in this domain are practically immobile in the membrane center. The bell-shaped profiles of membrane fluidity in these domains are inverted as compared to profiles in bulk lipids. All of these indicate that alkyl chains are strongly immobilized by the contact with

membrane proteins. Interestingly, membrane fluidity in the bulk domain increases toward the membrane center while, in the remaining domains, the membrane fluidity decreases toward the membrane center.

3.2.2. Saturation-recovery EPR—Fluidity profiles (T_1^{-1} versus depth in the membrane) obtained based on SR measurements for deoxygenated samples (see Fig. 3) are presented in Fig. 5A and B showing that one lipid domain in cortical and nuclear intact membranes has high fluidity and the other very low fluidity. The high fluidity profiles observed for cortical and nuclear intact membranes were similar to those obtained for human lens lipid membranes (also superimposed in Fig. 5) and were assigned to the bulk plus boundary lipids. Remaining profiles with the low spin-lattice relaxation rate were assigned to the trapped lipids. The bulk plus boundary domain and the trapped lipid domain can be discriminated with this method by all *n*-SASLs giving additional information about dynamics of alkyl chain of PLs in each domain without their physical separation.

The exchange rate between boundary and bulk lipids is of the order of magnitude of 10^7 s^{-1} or greater (East et al., 1985; Marsh, 1997; Ryba et al., 1987). This was the reason why boundary lipids were discriminated by the conventional EPR (Knowles et al., 1979; Marsh et al., 1982) (with the time window of the method from 100 ps to 10 ns) and not by the SR method of the discrimination by oxygen transport (Ashikawa et al., 1994a) (with the time window from 100 ns to 100 μs). Because the spin-lattice relaxation times of lipid spin labels in membranes are from 1 to 10 μs, the bulk and boundary domains cannot be discriminated by these measurements.

Three conclusions can be drawn from profiles in Fig. 5. (1) Alkyl chains are very immobile in the trapped lipids. T_1^{-1}s for *n*-SASLs in this domain are close to those in gel-phase membranes (Subczynski et al., 1990; Subczynski et al., 1989, 1991), indicating that membrane dynamics is suppressed to the level of gel-phase. (2) The lipid exchange rate between discriminated domains have to be smaller than the smallest spin-lattice relaxation rate of spin labels, which is 0.2×10^6 s^{-1} for the trapped domain (but see Sect. 3.3). (3) The alkyl chains in the trapped lipid domain are less mobile in the nucleus than in the cortex.

3.3. Membrane fluidity reported in terms of translational diffusion of molecular oxygen

Profiles of the OTP across cortical and nuclear fiber cell plasma membranes (Fig. 6A and B) also show that two domains can be discriminated. Because of the fast exchange rate of lipids between bulk and boundary domains, profiles with higher OTP were assigned to the bulk plus boundary domain (see (Ashikawa et al., 1994a) and discussion in Sect. 3.2.2). Comparison of these profiles with those presented for cortical and nuclear lens lipid membranes (profiles superimposed in Fig. 6) indicates that the effect of boundary lipids on the OTP is significantly greater in nucleus than in cortex. Values of the OTP in the center of the bulk plus boundary domain of the cortical and nuclear intact membrane are about 25% and 55% smaller than those in the center of the cortical and nuclear lens lipid membranes. Additionally, values of the OTP in the center of the nuclear intact membrane (Fig. 6B) are about 45% smaller than those in the cortical intact membrane (Fig. 6A). The presence of membrane proteins changes the shape of the profile to bell-shaped, with a gradual increase in the OTP from the membrane surface to its center. These bell-shaped profiles contrast with the rectangular profiles in lens lipid membranes with the ~3 times abrupt increase of the OTP between C9 and C10 positions on the alkyl chains. All of these changes are greater in nuclear membranes, in agreement with the greater amount of membrane proteins in the lens nucleus than in the lens cortex (Li et al., 1986; Li et al., 1985).

The remaining profiles in cortical (Fig. 6A) and nuclear (Fig. 6B) membranes were assigned to trapped lipids. The OTP values in this domain are extremely low, significantly lower than OTP values in the CBD (see superimposed profiles in Fig. 6), and comparable to those in gel-phase membranes (Subczynski et al., 1989). They are ~10 times lower than in water and ~20 times lower than in the center of the bulk plus boundary domain. This is in agreement with the extremely low mobility of alkyl chains in that domain indicated by profiles of the maximum splitting (Fig. 4) and by profiles of the T_1^{-1} (Fig. 5). We should note that profiles of the maximum splitting show averaged properties of the boundary and trapped lipid domains while profiles of the T_1^{-1} as well as profiles of the OTP reflect properties of the pure trapped lipid domain.

3.4. Discrimination of membrane domains using the cholesterol-analog spin label

The discrimination by oxygen transport method using ASL was applied here to show if the CBD, which was discriminated in lens lipid membranes (Mainali et al., 2013c), can be also detected in intact membranes. Spin-lattice relaxation rates of ASL (see Fig. 3B for their measurements) are included into profiles in Fig. 5. As a Chol analog, ASL can be located in all four purported domains in intact membranes, namely in bulk, boundary, and trapped lipids, as well as in the CBD. Due to the high exchange rate of lipids between boundary and bulk lipids (see Sect. 3.2.2) ASL cannot discriminate between these domains. Additionally, T_1^{-1}s of ASL in the bulk domain and in the CBD are similar (almost equal) (Raguz et al., 2011a, b). Thus, the high relaxation rate component in the ASL SR signal describes averaged mobility of Chol in these three domains (bulk, boundary, and CBD). The remaining slow relaxation rate component describes mobility of Chol in the trapped lipid domain. Since the nitroxide moiety is rigidly attached to the rigid ring structure of Chol in ASL (see Fig. 1), it senses membrane fluidity differently than *n*-SASLs. The latter describes segmental motion of alkyl chains while the former describes the motion of the whole rigid ring structure of Chol, which is located in the upper part of the hydrocarbon chains (to the depth of the C9). This is most likely the reason that ASL shows a bigger difference in fluidity between discriminated domains. Nevertheless, it is beneficial to monitor membrane fluidity sensed by PL and Chol analog spin labels.

Values of the OTP are obtained directly from SR measurements as an effect of oxygen on the components of the SR signal and are straightforward connected with components of the SR signal obtained without oxygen (Fig. 3B). Thus, the extremely low value of the OTP measured from the effect of oxygen on the slower value of the T_1^{-1} of ASL should be assigned to the trapped lipid domain. The remaining value comes from ASL in the bulk, boundary, and CBD. Presently, we have not been able to discriminate the CBD. Fitting the SR signals to three components and getting reasonable data is always a challenging problem. We hope that with the bigger sample and by using different experimental conditions, we will be able to overcome this problem.

Values of the OTP measured with ASL in more and less fluid domains of cortical and nuclear membranes are included into profiles in Fig. 6. Values measured in more fluid domain of cortical and nuclear membranes are significantly larger than those measured with *n*-SASLs at C10 positions (the nitroxide moiety of ASL is located at the depth of C10 in the membrane (Widomska et al., 2007a)), although they are still considerably smaller than those measured with ASL in lens lipids (Fig. 3B in (Mainali et al., 2013c)). The second value of the OTP measured with ASL is extremely low and falls into the profile across the trapped lipid domain. Although ASL discriminate the CBD in cortical and nuclear lens lipid membranes (Mainali et al., 2011b; Mainali et al., 2012a, 2013c; Raguz et al., 2008, 2009),

we have not yet been able to discriminate the CBD in intact membranes (Mainali et al., 2012a).

3.5. Hydrophobicity of membrane interior

Figure 7A and B shows hydrophobicity profiles across the lipid bilayer portion of intact cortical and nuclear lens membranes. Both profiles indicate the existence of a high hydrophobic barrier in intact lens membranes. The $2A_Z$ values in the center of both membranes (positions of 12- and 16-SASL) indicate that hydrophobicity in this region can be compared to that of N-butylamine and 1-decanol ($\varepsilon = 6–8$). Fig. 7 contains also superimposed profiles from cortical and nuclear lens lipid membranes, which allow concluding that the presence of proteins changes a rectangular hydrophobicity profile to one that is bell-shaped. The center of intact membranes becomes less hydrophobic than that of lens lipid membranes. The effect of membrane proteins on hydrophobicity profiles close to the membrane surface is rather negligible. Hence, the hydrophobicity of the membrane center is lowered by the presence of membrane proteins, although this is still a considerably high hydrophobic barrier, which ensures that the transport of water, ions, and other small polar and ionic molecules is tightly controlled by membrane proteins. Because $2A_Z$ values were measured for a frozen membrane suspension (see Fig. 2C and D and Sect. 2.5), the EPR spectrum is the superposition of individual spectra from all domains reporting averaged membrane hydrophobicity.

3.6. Permeability of oxygen across membrane domains

Based on profiles of the OTP across the bulk plus boundary domain and trapped lipid domain in intact cortical and nuclear membranes presented in Figs. 6A and B, and procedure described in Sect. 2.6, permeability coefficients for oxygen across these domains were evaluated. They are listed in the Table 1 together with values obtained for lipid domains in cortical and nuclear lens lipid membranes. This allows us to elucidate only the effect of proteins on oxygen transport across domains, because the effect of the high Chol content is already included in the permeability of lens lipid membranes. The high protein content in fiber cell plasma membranes strongly decreases the oxygen permeability across the lipid bilayer portion of these membranes. The permeability of the bulk plus boundary domain in the cortical and nuclear membrane is, respectively, 13 and 25% lower than across the bulk lipids in cortical and nuclear lens lipid membranes. The permeability of the bulk plus boundary domain in the nuclear membrane is 23% lower than that across the bulk plus boundary domain in the cortical membrane. This indicates that the contribution of boundary lipids to the permeability property is greater in nuclear membranes. Similarly, permeability of trapped lipids in the nuclear membrane is about 50% smaller that that in the cortical membrane. This can be explained also by the greater rigidity of trapped lipids in the nuclear membrane (but see Sect. 3.7). The permeability for oxygen across this domain is not only smaller than across the CBD (see Table 1) but even smaller than across gel-phase membranes (Subczynski et al., 1989).

3.7. Amount of lipids in lipid domains

In the paper on intact porcine eye lens membranes, we showed that the effect of membrane proteins on the lipid bilayer portion of the membrane is greater in nucleus than in cortex (Mainali et al., 2012a). Here, for human lenses, we made an attempt to evaluate relative amounts of lipids in the domains discriminated in intact membranes.

Based on the EPR spectrum of 12-SASL (PL analog spin label), which is the superposition of the spectrum coming from bulk PLs and the spectrum coming from boundary plus trapped PLs, we evaluated the relative amount of the bulk PLs. Based on the SR EPR signal of 12-SASL, that is the superposition of the signal coming from bulk plus boundary PLs and

from trapped PLs, we were able to assess the relative amount of trapped PLs. Figure 2B, E, and F illustrates the procedure for the evaluation of the amount of PLs in the bulk domain. The EPR spectrum of 12-SASL in cortical intact membranes (A) and the EPR spectrum of 12-SASL in cortical lens lipid membranes (B) ((B) is a bulk component in spectrum (A)) are experimental spectra. The spectrum (C) is also the experimental spectrum of 12-SASL in the cortical lens lipid membrane obtained at decreased temperature to get the spectrum with the same maximum splitting as that for the strongly immobilized component in spectrum (A) (value taken from Fig. 4). The spectrum (C) should approximate the spectrum coming from the boundary plus trapped PLs with the motion decreased to almost rigid limit conditions. The spectrum (A) can be successfully reproduced by adding 63% of spectrum (B) and 37% of spectrum (C), where 100% of spectrum (B) and (C) indicates spectra with the same intensity (the same surface under the absorption curve). Thus, in cortical membranes the amount of PLs in domains uniquely formed due to the presence of membrane proteins accounts for 37% of total PLs. A similar procedure was performed for nuclear membranes indicating that the relative abundant of PLs in domains formed due to the presence of membrane proteins is 46%, thus significantly greater than in cortical membranes. The precision of this estimation is better than 5%, because a 5% change in the contribution of each component decreases the goodness of the fit.

Figure 8 illustrates the procedure for the evaluation of the amount of PLs in the bulk plus boundary domain and in the trapped domain which is based on the SR measurements. The SR signal of 12-SASL in intact membranes (A) can be successfully simulated by the double exponential curve, indicating that spin labels are located in two environments with different fluidity. As described in Sect. 3.2.2, we assigned the signal with the shorter T_1 (signal (B)) as coming from bulk plus boundary PLs and with longer T_1 (signal (C)) as coming from trapped PLs. The contribution of each component to the experimental signal is given by the pre-exponential factor obtained from the fitting program. Because the SR signal is recorded with the delay (in our case 2.2 μs), after the end of the saturating pulse, we have to extrapolate back the exponentials for each component to get actual ratio of their pre-exponential coefficients. This procedure is also illustrated in Fig. 8. Pre-exponential coefficients for 12-SASL in cortical and nuclear membranes indicate that the abundance of trapped PLs in these membranes is, respectively, 36 and 51%. All of these data describing distribution of PLs between membrane domains are included in Table 2.

The relative distribution of Chol is indicated by the distribution of Chol analog, ASL (Fig. 1). We performed similar evaluations, as illustrated in Fig. 2B, E, and F, based on conventional EPR spectra of ASL in intact cortical and nuclear membranes (Fig.2G and H). Because EPR spectra of ASL coming from bulk lipids and from CBD are similar (Mainali et al., 2012b; Raguz et al., 2011a, b), the only explanation of these results is that in cortical membranes ASL is located only in bulk lipids and CBDs (see also Discussion). This data also suggests that the amount of ASL in trapped lipids is negligible (not detectable by conventional EPR). However, based on the analysis of the SR signals from ASL (Fig. 3B) and using the same procedure as illustrated in Fig. 8, we evaluated the relative amount of Chol (ASL) in the cortical trapped domain as 23%. The amount of Chol in trapped lipids in nuclear membranes is ~50% (as deduced from the conventional EPR spectra of ASL (Fig. 2H)) and 46% (as deduced from the SR measurements). All of these data dealing with the distribution of Chol are included in Table 3. All these approaches indicated that the relative amount of lipids (PLs and Chol) in domains formed due to the presence of membrane proteins is greater in nuclear membranes as compared with cortical membranes.

4. Discussion

Figure 9 is a schematic drawing that illustrates the presence of the four purported lipid domains in intact fiber cell membranes of the human eye lens. In the described research, we were able to confirm existence of the three of them, namely bulk, boundary, and trapped lipid domains. However, we have not been able to discriminate the CBD, which was easily discriminated in cortical and nuclear lens lipid membranes (Mainali et al., 2013c). In the presented research, we also made effort to quantitatively evaluate the relative amounts of PLs and Chol in lipid domains in intact human eye lens membranes (Tables 2 and 3). Based on conventional EPR spectra of 12-SASL, we showed that lipid domains formed due to the presence of membrane proteins, namely boundary and trapped lipid domains, account, respectively, for 37 and 46% of total PLs in cortical and nuclear membranes. SR EPR measurements with 12-SASL, which discriminate trapped PLs from bulk plus boundary PLs, indicate that trapped PLs account, respectively, for 36 and 51% of total PLs in cortical and nuclear membranes. Conventional EPR spectra of ASL indicate virtually total exclusion of Chol from lipid domains formed due to the presence of membrane proteins in cortical intact membranes. However, in nuclear membranes, about 50% of Chol is located in the protein induced lipid domains. This phenomenon was repeatedly observed in lenses from different species (Mainali et al., 2012a) and in human lenses from donors of different ages (from 0- to 20-year-old and from 21- to 40-year-old donors, data not shown). This surprising result can be partly explained with the assumption that in intact fiber cell membranes of the human eye lens Chol and ASL are substantially excluded from the boundary lipids around integral proteins. The exclusion of these molecules from boundary layers was observed using different techniques and for different systems including erythrocyte membrane (Aloni et al., 1977; Bieri and Wallach, 1975), high density lipoprotein recombinants (Dergunov et al., 1997; Massey et al., 1984; Tall and Lange, 1978), or sarcoplasmic reticulum ATPase (Warren et al., 1975). Thus, our assumption, which is already incorporated in Fig. 9, seems reasonable. SR EPR with ASL showed that the trapped lipid domain accounts, respectively, for 23% and 45% of total Chol in cortical and nuclear membranes. It is significant that all these different EPR approaches show the same tendency in changes in the amounts of lipids in membrane domains. All these new approaches will allow quantitatively evaluate changes in the organization of lipids in intact fiber cell membranes occurring with age and with cataract formation.

Formation of boundary and/or trapped lipids is likely induced by aquaporin-0 (AQP0) and connexins (Cx46 and Cx50) (Gonen et al., 2005; Reichow and Gonen, 2009), the most abundant proteins in the human lens fiber cell membrane (Bassnett et al., 2011). These proteins belong to two major classes of fiber cell integral transmembrane proteins that perform the communication between fiber cells. AQP0, which belongs to the water transport family of integral channel proteins, controls transport of water and some neutral solutes, but not ions (Agre, 2004). The second class belongs to connexins, Cx46 and Cx50 (with Cx46 found mainly in the cortex and outer nuclear layers and Cx50 found mainly in the nuclear core (Chung et al., 2007; Tenbroek et al., 1992; White et al., 1998)), which form gap junctions between lens fiber cells (Mathias et al., 2010). Exchange of ions and small metabolites (glucose, amino acids) between lens cells depend on these gap junctions (Mathias et al., 2010). These proteins form ordered two-dimensional arrays in fiber cell membranes (Buzhynskyy et al., 2007; Buzhynskyy et al., 2011; Costello et al., 1989; Dunia et al., 2006; Gonen et al., 2004; Zampighi et al., 2002) and lipids can be trapped within these protein-dense structures. Interestingly, the density/distribution of these proteins varies as a function of fiber depth (age) (Kuszak et al., 2004) and the ordered arrays of AQP0 are enriched in the nucleus (Costello et al., 1989). This is consistent with our current data, which show that the amount of trapped lipids and the extent of lipid rigidity are greater in the nucleus than in the cortex. Both the amount of protein and the packing of protein in

membranes might be important in modifying the observed physical properties of lipid bilayer and the distribution of lipids between membrane domains.

The unexpected distribution of Chol in the cortical fiber cell membranes can, to a certain degree, be also explained by the data presented by Lo and co-authors (Biswas et al., 2009; Biswas et al., 2010; Biswas and Lo, 2007), showing that the significant structural remodeling of gap junctions takes place during fiber cell development and maturation. Gap junctions are selectively localized within the specialized interlocking membrane domains between lens fibers called “ball-and-sockets” (Biswas et al., 2010). The newly formed gap junction channels in the superficial young fiber cells are continuously clustered, forming large Chol-rich loosely-packed gap junction plagues. In the matured inner cortical fibers they are transformed into Chol-free tightly-packed clusters (Biswas et al., 2009; Biswas and Lo, 2007). This explains why in cortical membranes the relative amount of Chol trapped between membrane proteins is small (close to zero when measured using conventional EPR and as small as 23% when measured using SR EPR). In nuclear membranes, which are enriched in ordered arrays of AQP0, amounts of trapped lipids, including trapped Chol is greater (Table 2).

Data presented in Table 1 indicate that for all membrane domains discriminated with EPR spin-labeling methods in human intact cortical and nuclear fiber cell membranes, the permeability for oxygen is significantly lower than across water layers of the same thickness as these domains. This effect is mainly due to the presence of membrane proteins and formation of boundary and trapped lipid domains. Permeability of cortical and nuclear lens lipid membranes (membranes without proteins) is comparable to those across water layers of the same thickness (Table 2 in (Mainali et al., 2013c)). Permeability of the bulk plus boundary domain in cortical and nuclear membranes is, respectively, 30 and 43% smaller than across water layers of the same thickness as the domain. This difference is much greater for trapped lipids in cortical and nuclear membranes, which show permeability, respectively, 5.6 and 11 times smaller than across water layers of the same thickness. Because trapped lipids in cortical and nuclear membranes account, respectively, for 36 and 51% of total lipids (data for SR measurements with 12-SASL taken from Table 2), their contribution to the formation of the barrier to oxygen transport is substantial, especially in the lens nucleus. The results reported here complement our studies on the oxygen permeability across lens lipid membranes summarized in the Review (Subczynski et al., 2012) and across intact fiber cell plasma membranes isolated from porcine eyes (Mainali et al., 2012a).

Organization of membrane proteins is a significant factor that determines the organization and properties of the lipid bilayer portion of fiber-cell membranes of human lenses. We would like to add some comments on how the unique lipid composition of these membranes, which includes a high content of saturated sphingolipids (Byrdwell and Borchman, 1997; Byrdwell et al., 1994; Huang et al., 2005) and only traces of polyunsaturated fatty acids (Broekhuyse and Soeting, 1976; Zelenka, 1978), may contribute to the lipid-protein interactions. The flexible saturated alkyl chains can fit easier to the protein surface than unsaturated alkyl chains with a rigid *cis* double bond, which introduce a bend of 30° at that bond. The high level of saturation ensures the highest packing density of membrane components. The tightly packed chains preserve their randomly bended structures, but they become “glued” to the surface of transmembrane proteins, which minimized their thermal motion. Thus, the rigidity of the lipid bilayer portion of fiber cell membranes is achieved mainly by decreased dynamics of alkyl chains, and not by their ordering. With that explanation, our results are not in contrast with those presented by Sato et al. (Sato et al., 1996) and Zhang et al.(Zhang et al., 1999), which showed that the structural order determined by the static measure of the *trans/gauche* rotamer ratio in the hydrocarbon

chains of bovine and human lens membranes is not affected by the presence of intrinsic and extrinsic lens proteins. These static and dynamic descriptions of membrane properties complement each other, concluding that at the high protein concentration alkyl chains of PLs fill up the space between proteins accepting all necessary bending structures, although their motion is frozen by the tight protein packing.

The studies reported here were carried out at X-band EPR spectrometers with a loop-gap resonator that has a sample volume of 3 μL. To complete all measurements and obtain detailed profiles, samples were isolated from about 20 lenses and pooled. It is not difficult to obtain these numbers of similar lenses (age is the major criterion) from a meat-packing plant. Human lenses however are more precious and more difficult to obtain in these numbers from eye banks. A more serious problem is that human lenses can be different not only because of age, but also because of varying health history of the donor. The best solution of this problem will be to perform all measurements on samples prepared from one or two lenses from a single donor. Recently, we demonstrated the feasibility of such measurements, showing that profiles of membrane properties can be obtained at W-band with the loop-gap resonator with a sample volume of 30 nL (Mainali et al., 2013b; Mainali et al., 2011b). Thus, theoretically, the total amount of sample can be 100 times smaller at W-band than at X-band. However, handling of the sample with the present design, especially equilibration with nitrogen and air has to be performed outside the resonator for much larger (about 3 μL) sample volume. We are now in the process of overcoming these problems. Presently, we were able to make three repetitions of our experiments with three different preparations of cortical and nuclear membranes from three pairs of lenses from different donors, but only for one experimental point (one spin label). We chose 12-SASL which not only allowed us to confirm validity of appropriate points in profiles of membrane properties (data included in captions of Figs. 4–7), but also confirm validity of the data about amounts of PLs in domains uniquely formed due to the presence of membrane proteins (data included into Table 2). However information unique to an individual lens is muted when data averaging and pooling samples is required. We believe that all of these new methods, which allow for the quantification of lipid domains in intact fiber cell membranes, combined with the measurements of samples from a single donor, have the potential to be a powerful approach for studying changes in fiber cell membranes occurring with age and with cataract formation.

Acknowledgments

This work was supported by grants EY015526, EB002052, EB001980, and EY001931, and a construction grant, RR016511, from the National Institutes of Health. Ivana Krpan assisted during sample preparations and EPR measurements.

References

Agre P. Nobel Lecture. Aquaporin water channels. Biosci. Rep. 2004; 24:127–163. [PubMed: 16209125]

Aloni B, Eitan A, Livne A. The erythrocyte membrane site for the effect of temperature on osmotic fragility. Biochim. Biophys. Acta. 1977; 465:46–53. [PubMed: 836832]

Ashikawa I, Yin J-J, Subczynski WK, Kouyama T, Hyde JS, Kusumi A. Molecular organization and dynamics in bacteriorhodopsin-rich reconstituted membranes: discrimination of lipid environments by the oxygen transport parameter using a pulse ESR spin-labeling technique. Biochemistry (Mosc). 1994a; 33:4947–4952.

Ashikawa I, Yin JJ, Subczynski WK, Kouyama T, Hyde JS, Kusumi A. Molecular organization and dynamics in bacteriorhodopsin-rich reconstituted membranes: discrimination of lipid environments by the oxygen transport parameter using a pulse ESR spin-labeling technique. Biochemistry. 1994b; 33:4947–4952. [PubMed: 8161556]

Bassnett S, Beebe DC. Coincident loss of mitochondria and nuclei during lens fiber cell differentiation. Developmental dynamics : an official publication of the American Association of Anatomists. 1992; 194:85–93. [PubMed: 1421526]

Bassnett S, Shi Y, Vrensen GF. Biological glass: structural determinants of eye lens transparency. Philosophical transactions of the Royal Society of London. Series B, Biological sciences. 2011; 366:1250–1264.

Beebe, DC. The lens. In: Kaufman, PL., editor. Physiology of the eye. St Louis: Mosby-Year Book; 2003. p. 117-158.

Bieri VG, Wallach DF. Variations of lipid-protein interactions in erythrocyte ghosts as a function of temperature and pH in physiological and non-physiological ranges. A study using a paramagnetic quenching of protein fluorescence by nitroxide lipid analogues. Biochim. Biophys. Acta. 1975; 406:415–423. [PubMed: 241415]

Biswas SK, Jiang JX, Lo WK. Gap junction remodeling associated with cholesterol redistribution during fiber cell maturation in the adult chicken lens. Mol. Vis. 2009; 15:1492–1508. [PubMed: 19657477]

Biswas SK, Lee JE, Brako L, Jiang JX, Lo WK. Gap junctions are selectively associated with interlocking ball-and-sockets but not protrusions in the lens. Mol. Vis. 2010; 16:2328–2341. [PubMed: 21139982]

Biswas SK, Lo WK. Gap junctions contain different amounts of cholesterol which undergo unique sequestering processes during fiber cell differentiation in the embryonic chicken lens. Mol. Vis. 2007; 13:345–359. [PubMed: 17392685]

Bloemendal H, Zweers A, Vermorken F, Dunia I, Benedetti EL. The plasma membranes of eye lens fibres. Biochemical and structural characterization. Cell Differ. 1972; 1:91–106. [PubMed: 4275925]

Borchman D, Byrdwell WC, Yappert MC. Regional and age-dependent differences in the phospholipid composition of human lens membranes. Invest. Ophthalmol. Vis. Sci. 1994; 35:3938–3942. [PubMed: 7928192]

Borchman D, Yappert MC. Lipids and the ocular lens. J. Lipid Res. 2010; 51:2473–2488. [PubMed: 20407021]

Broekhuyse RM, Soeting WJ. Lipids in tissues of the eye. XV. Essential fatty acids in lens lipids. Exp. Eye Res. 1976; 22:653–657. [PubMed: 776644]

Budil DE, Lee S, Saxena S, Freed JH. Nonlinear-Least-Squares Analysis of Slow-Motion EPR Spectra in One and Two Dimensions Using a Modified Levenberg-Marquardt Algorithm. Journal of Magnetic Resonance, Series A. 1996; 120:155–189.

Buzhynskyy N, Hite RK, Walz T, Scheuring S. The supramolecular architecture of junctional microdomains in native lens membranes. EMBO Rep. 2007; 8:51–55. [PubMed: 17124511]

Buzhynskyy N, Sens P, Behar-Cohen F, Scheuring S. Eye lens membrane junctional microdomains: a comparison between healthy and pathological cases. New J. Phys. 2011; 13:1–16.

Byrdwell WC, Borchman D. Liquid chromatography/mass-spectrometric characterization of sphingomyelin and dihydrosphingomyelin of human lens membranes. Ophthalmic Res. 1997; 29:191–206. [PubMed: 9261843]

Byrdwell WC, Borchman D, Porter RA, Taylor KG, Yappert MC. Separation and characterization of the unknown phospholipid in human lens membranes. Invest. Ophthalmol. Vis. Sci. 1994; 35:4333–4343. [PubMed: 8002253]

Cenedella RJ, Fleschner CR. Selective association of crystallins with lens 'native' membrane during dynamic cataractogenesis. Curr Eye Res. 1992; 11:801–815. [PubMed: 1424724]

Chandrasekher G, Cenedella RJ. Protein associated with human lens 'native' membrane during aging and cataract formation. Experimental eye research. 1995; 60:707–717. [PubMed: 7641853]

Chung J, Berthoud VM, Novak L, Zoltoski R, Heilbrunn B, Minogue PJ, Liu X, Ebihara L, Kuszak J, Beyer EC. Transgenic overexpression of connexin50 induces cataracts. Exp. Eye Res. 2007; 84:513–528. [PubMed: 17217947]

Costello MJ, McIntosh TJ, Robertson JD. Distribution of gap junctions and square array junctions in the mammalian lens. Invest. Ophthalmol. Vis. Sci. 1989; 30:975–989. [PubMed: 2722452]

Dahm R. Lens fibre cell differentiation - A link with apoptosis? Ophthalmic Res. 1999; 31:163–183. [PubMed: 10224500]

Dahm R, van Marle J, Quinlan RA, Prescott AR, Vrensen GF. Homeostasis in the vertebrate lens: mechanisms of solute exchange. Philosophical transactions of the Royal Society of London. Series B, Biological sciences. 2011; 366:1265–1277.

Deeley JM, Mitchell TW, Wei X, Korth J, Nealon JR, Blanksby SJ, Truscott RJ. Human lens lipids differ markedly from those of commonly used experimental animals. Biochim. Biophys. Acta. 2008; 1781:288–298. [PubMed: 18474264]

Dergunov AD, Taveirne J, Vanloo B, Caster H, Rosseneu M. Structural organization of lipid phase and protein-lipid interface in apolipoprotein-phospholipid recombinants: influence of cholesterol. Biochim. Biophys. Acta. 1997; 1346:131–146. [PubMed: 9219896]

Dunia I, Cibert C, Gong X, Xia CH, Recouvreur M, Levy E, Kumar N, Bloemendal H, Benedetti EL. Structural and immunocytochemical alterations in eye lens fiber cells from Cx46 and Cx50 knockout mice. Eur. J. Cell Biol. 2006; 85:729–752. [PubMed: 16740340]

East JM, Melville D, Lee AG. Exchange rates and numbers of annular lipids for the calcium and magnesium ion dependent adenosinetriphosphatase. Biochemistry (Mosc). 1985; 24:2615–2623.

Epand, RM. Role of membrane lipids in modulating the activity of membrane-bound enzymes. In: Yeagle, PL., editor. The structure of biological membrane. Boca Raton: CRC Press; 2005. p. 499-509.

Estrada R, Puppato A, Borchman D, Yappert MC. Reevaluation of the phospholipid composition in membranes of adult human lenses by (31)P NMR and MALDI MS. Biochim. Biophys. Acta. 2010; 1798:303–311. [PubMed: 19925778]

Estrada R, Yappert MC. Regional phospholipid analysis of porcine lens membranes by matrix-assisted laser desorption/ionization time-of-flight mass spectrometry. J. Mass Spectrom. 2004; 39:1531–1540. [PubMed: 15578747]

Folch J, Lees M, Sloane Stanley GH. A simple method for the isolation and purification of total lipids from animal tissues. J. Biol. Chem. 1957; 226:497–509. [PubMed: 13428781]

Gonen T, Cheng Y, Kistler J, Walz T. Aquaporin-0 membrane junctions form upon proteolytic cleavage. J. Mol. Biol. 2004; 342:1337–1345. [PubMed: 15351655]

Gonen T, Cheng Y, Sliz P, Hiroaki Y, Fujiyoshi Y, Harrison SC, Walz T. Lipid-protein interactions in double-layered two-dimensional AQP0 crystals. Nature. 2005; 438:633–638. [PubMed: 16319884]

Griffith, OH.; Jost, PC. Lipid Spin Labels in Biological Membranes. In: Berliner, LJ., editor. Spin Labeling Theory and Applications. New York, San Francisco, London: Academic Press; 1976. p. 453-523.

Huang L, Grami V, Marrero Y, Tang D, Yappert MC, Rasi V, Borchman D. Human lens phospholipid changes with age and cataract. Invest. Ophthalmol. Vis. Sci. 2005; 46:1682–1689. [PubMed: 15851569]

Hubbell WL, McConnell HM. Spin-label studies of the excitable membranes of nerve and muscle. Proc. Natl. Acad. Sci. U. S. A. 1968; 61:12–16. [PubMed: 4301585]

Hughes JR, Deeley JM, Blanksby SJ, Leisch F, Ellis SR, Truscott RJ, Mitchell TW. Instability of the cellular lipidome with age. Age (Dordr). 2012; 34:935–947. [PubMed: 21894448]

Jost PC, Griffith OH, Capaldi RA, Vanderkooi G. Evidence for boundary lipid in membranes. Proc. Natl. Acad. Sci. U. S. A. 1973; 70:480–484. [PubMed: 4346892]

Kawasaki K, Yin J-J, Subczynski WK, Hyde JS, Kusumi A. Pulse EPR detection of lipid exchange between protein rich raft and bulk domains in the membrane: methodology development and its application to studies of influenza viral membrane. Biophys. J. 2001; 80:738–748. [PubMed: 11159441]

Kistler J, Bullivant S. Lens gap junctions and orthogonal arrays are unrelated. FEBS Lett. 1980; 111:73–78. [PubMed: 7358167]

Knowles PF, Watts A, Marsh D. Spin-label studies of lipid immobilization in dimyristoylphosphatidylcholine-substituted cytochrome oxidase. Biochemistry (Mosc). 1979; 18:4480–4487.

Kusumi A, Subczynski WK, Hyde JS. Oxygen transport parameter in membranes as deduced by saturation recovery measurements of spin-lattice relaxation times of spin labels. Proc. Natl. Acad. Sci. U. S. A. 1982; 79:1854–1858. [PubMed: 6952236]

Kusumi A, Subczynski WK, Pasenkiewicz-Gierula M, Hyde JS, Merkle H. Spin-label studies on phosphatidylcholine-cholesterol membranes: effects of alkyl chain length and unsaturation in the fluid phase. Biochim. Biophys. Acta. 1986; 854:307–317. [PubMed: 3002470]

Kuszak JR, Zoltoski RK, Tiedemann CE. Development of lens sutures. The International journal of developmental biology. 2004; 48:889–902. [PubMed: 15558480]

Li LK, Roy D, Spector A. Changes in lens protein in concentric fractions from individual normal human lenses. Curr. Eye Res. 1986; 5:127–135. [PubMed: 3956240]

Li LK, So L. Age dependent lipid and protein changes in individual bovine lenses. Curr. Eye Res. 1987; 6:599–605. [PubMed: 3581878]

Li LK, So L, Spector A. Membrane cholesterol and phospholipid in consecutive concentric sections of human lenses. J. Lipid Res. 1985; 26:600–609. [PubMed: 4020298]

Li LK, So L, Spector A. Age-dependent changes in the distribution and concentration of human lens cholesterol and phospholipids. Biochim. Biophys. Acta. 1987; 917:112–120. [PubMed: 3790601]

Ligeza A, Tikhonov AN, Hyde JS, Subczynski WK. Oxygen permeability of thylakoid membranes: electron paramagnetic resonance spin labeling study. Biochim. Biophys. Acta. 1998; 1365:453–463. [PubMed: 9711298]

Lim J, Lam YC, Kistler J, Donaldson PJ. Molecular characterization of the cystine/glutamate exchanger and the excitatory amino acid transporters in the rat lens. Invest Ophthalmol Vis Sci. 2005; 46:2869–2877. [PubMed: 16043861]

Mailer C, Nielsen RD, Robinson BH. Explanation of spin-lattice relaxation rates of spin labels obtained with multifrequency saturation recovery EPR. The journal of physical chemistry. A. 2005; 109:4049–4061. [PubMed: 16833727]

Mainali L, Feix JB, Hyde JS, Subczynski WK. Membrane fluidity profiles as deduced by saturation-recovery EPR measurements of spin-lattice relaxation times of spin labels. J. Magn. Reson. B. 2011a; 212:418–425.

Mainali L, Hyde JS, Subczynski WK. Using spin-label W-band EPR to study membrane fluidity profiles in samples of small volume. J. Magn. Reson. B. 2013a; 226:35–44.

Mainali L, Hyde JS, Subczynski WK. Using spin-label W-band EPR to study membrane fluidity profiles in samples of small volume. J. Magn. Reson. 2013b; 226:35–44. [PubMed: 23207176]

Mainali L, Raguz M, Camenisch TG, Hyde JS, Subczynski WK. Spin-label saturation-recovery EPR at W-band: applications to eye lens lipid membranes. J. Magn. Reson. B. 2011b; 212:86–94.

Mainali L, Raguz M, O'Brien WJ, Subczynski WK. Properties of fiber cell plasma membranes isolated from the cortex and nucleus of the porcine eye lens. Exp. Eye Res. 2012a; 97:117–129. [PubMed: 22326289]

Mainali L, Raguz M, O'Brien WJ, Subczynski WK. Properties of membranes derived from the total lipids extracted from the human lens cortex and nucleus. Biochim. Biophys. Acta. 2013c; 1828:1432–1440. [PubMed: 23438364]

Mainali L, Raguz M, Subczynski WK. Phases and domains in sphingomyelin-cholesterol membranes: structure and properties using EPR spin-labeling methods. Eur. Biophys. J. 2012b; 41:147–159. [PubMed: 22033879]

Marsh D. Stoichiometry of lipid-protein interaction and integral membrane protein structure. European biophysics journal : EBJ. 1997; 26:203–208.

Marsh D. Electron spin resonance in membrane research: protein-lipid interactions. Methods. 2008; 46:83–96. [PubMed: 18672066]

Marsh D. Electron spin resonance in membrane research: protein-lipid interactions from challenging beginnings to state of the art. European biophysics journal : EBJ. 2010; 39:513–525. [PubMed: 19669751]

Marsh D, Watts A, Pates RD, Uhl R, Knowles PF, Esmann M. ESR spin-label studies of lipid-protein interactions in membranes. Biophys. J. 1982; 37:265–274. [PubMed: 6275924]

Mason R, Tulenko TN, Jacob RF. Direct evidence for cholesterol crystalline domains in biological membranes: role in human pathobiology. Biochim. Biophys. Acta. 2003; 1610:198–207. [PubMed: 12648774]

Massey JB, Gotto AM Jr, Pownall HJ. Thermodynamics of lipid-protein association. Enthalphy of association of apolipoprotein A-II with dimyristoylphosphatidylcholine-cholesterol mixtures. Biochim. Biophys. Acta. 1984; 794:137–141. [PubMed: 6428456]

Mathias RT, White TW, Gong X. Lens gap junctions in growth, differentiation, and homeostasis. Physiol. Rev. 2010; 90:179–206. [PubMed: 20086076]

Paterson CA, Zeng J, Husseini Z, Borchman D, Delamere NA, Garland D, Jimenez-Asensio J. Calcium ATPase activity and membrane structure in clear and cataractous human lenses. Curr. Eye Res. 1997; 16:333–338. [PubMed: 9134322]

Rafferty, NS. Lens morphology. In: Maisel, H., editor. The ocular lens:structure, function and pathology. New York: Marcel Dekker; 1985. p. 1-60.

Raguz M, Mainali L, Widomska J, Subczynski WK. The immiscible cholesterol bilayer domain exists as an integral part of phospholipid bilayer membranes. Biochim. Biophys. Acta. 2011a; 1808:1072–1080. [PubMed: 21192917]

Raguz M, Mainali L, Widomska J, Subczynski WK. Using spin-label electron paramagnetic resonance (EPR) to discriminate and characterize the cholesterol bilayer domain. Chem. Phys. Lipids. 2011b; 164:819–829. [PubMed: 21855534]

Raguz M, Widomska J, Dillon J, Gaillard ER, Subczynski WK. Characterization of lipid domains in reconstituted porcine lens membranes using EPR spin-labeling approaches. Biochim. Biophys. Acta. 2008; 1778:1079–1090. [PubMed: 18298944]

Raguz M, Widomska J, Dillon J, Gaillard ER, Subczynski WK. Physical properties of the lipid bilayer membrane made of cortical and nuclear bovine lens lipids: EPR spin-labeling studies. Biochim. Biophys. Acta. 2009; 1788:2380–2388. [PubMed: 19761756]

Reichow SL, Gonen T. Lipid-protein interactions probed by electron crystallography. Curr. Opin. Struct. Biol. 2009; 19:560–565. [PubMed: 19679462]

Robinson BH, Haas DA, Mailer C. Molecular dynamics in liquids: spin-lattice relaxation of nitroxide spin labels. Science. 1994; 263:490–493. [PubMed: 8290958]

Rujoi M, Estrada R, Yappert MC. In situ MALDI-TOF MS regional analysis of neutral phospholipids in lens tissue. Anal. Chem. 2004; 76:1657–1663. [PubMed: 15018564]

Rujoi M, Jin J, Borchman D, Tang D, Yappert MC. Isolation and lipid characterization of cholesterol-enriched fractions in cortical and nuclear human lens fibers. Invest. Ophthalmol. Vis. Sci. 2003; 44:1634–1642. [PubMed: 12657603]

Ryba NJ, Horvath LI, Watts A, Marsh D. Molecular exchange at the lipid-rhodopsin interface: spin-label electron spin resonance studies of rhodopsin-dimyristoylphosphatidylcholine recombinants. Biochemistry (Mosc). 1987; 26:3234–3240.

Sato H, Borchman D, Ozaki Y, Lamba OP, Byrdwell WC, Yappert MC, Paterson CA. Lipid-protein interactions in human and bovine lens membranes by Fourier transform Raman and infrared spectroscopies. Exp. Eye Res. 1996; 62:47–53. [PubMed: 8674512]

Schreier S, Polnaszek CF, Smith IO. Spin labels in membranes. Problems in practice. Biochim. Biophys. Acta. 1978; 515:395–436. [PubMed: 215206]

Subczynski WK, Antholine WE, Hyde JS, Kusumi A. Microimmiscibility and three-dimensional dynamic structures of phosphatidylcholine-cholesterol membranes: translational diffusion of a copper complex in the membrane. Biochemistry (Mosc). 1990; 29:7936–7945.

Subczynski WK, Felix CC, Klug CS, Hyde JS. Concentration by centrifugation for gas exchange EPR oximetry measurements with loop-gap resonators. J. Magn. Reson. 2005; 176:244–248. [PubMed: 16040261]

Subczynski WK, Hopwood LE, Hyde JS. Is the mammalian cell plasma membrane a barrier to oxygen transport? J. Gen. Physiol. 1992; 100:69–87. [PubMed: 1324973]

Subczynski WK, Hyde JS, Kusumi A. Oxygen permeability of phosphatidylcholine-cholesterol membranes. Proc. Natl. Acad. Sci. U. S. A. 1989; 86:4474–4478. [PubMed: 2543978]

Subczynski WK, Hyde JS, Kusumi A. Effect of alkyl chain unsaturation and cholesterol intercalation on oxygen transport in membranes: a pulse ESR spin labeling study. Biochemistry (Mosc). 1991; 30:8578–8590.

Subczynski WK, Lewis RN, McElhaney RN, Hodges RS, Hyde JS, Kusumi A. Molecular organization and dynamics of 1-palmitoyl-2-oleoylphosphatidylcholine bilayers containing a transmembrane alpha-helical peptide. Biochemistry (Mosc). 1998; 37:3156–3164.

Subczynski WK, Raguz M, Widomska J. Studying lipid organization in biological membranes using liposomes and EPR spin labeling. Methods Mol. Biol. 2010; 606:247–269. [PubMed: 20013402]

Subczynski WK, Raguz M, Widomska J, Mainali L, Konovalov A. Functions of cholesterol and the cholesterol bilayer domain specific to the fiber-cell plasma membrane of the eye lens. J. Membr. Biol. 2012; 245:51–68. [PubMed: 22207480]

Subczynski WK, Widomska J, Feix JB. Physical properties of lipid bilayers from EPR spin labeling and their influence on chemical reactions in a membrane environment. Free Radic. Biol. Med. 2009; 46:707–718. [PubMed: 19111611]

Subczynski, WK.; Widomska, J.; Wisniewska, A.; Kusumi, A. Saturation-recovery electron paramagnetic resonance discrimination by oxygen transport (DOT) method for characterizing membrane domains. In: McIntosh, TJ., editor. Methods in Molecular Biology, Lipid Rafts. Totowa: Humana Press; 2007. p. 143-157.

Subczynski WK, Wisniewska A, Yin J-J, Hyde JS, Kusumi A. Hydrophobic barriers of lipid bilayer membranes formed by reduction of water penetration by alkyl chain unsaturation and cholesterol. Biochemistry (Mosc). 1994; 33:7670–7681.

Tall AR, Lange Y. Interaction of cholesterol, phospholipid and apoprotein in high density lipoprotein recombinants. Biochim. Biophys. Acta. 1978; 513:185–197. [PubMed: 214114]

Tenbroek E, Arneson M, Jarvis L, Louis C. The distribution of the fiber cell intrinsic membrane proteins MP20 and connexin46 in the bovine lens. J. Cell Sci. 1992; 103(Pt 1):245–257. [PubMed: 1331134]

Tong J, Briggs Margaret M, McIntosh Thomas J. Water Permeability of Aquaporin-4 Channel Depends on Bilayer Composition, Thickness, and Elasticity. Biophys. J. 2012; 103:1899–1908. [PubMed: 23199918]

Tong J, Canty JT, Briggs MM, McIntosh TJ. The water permeability of lens aquaporin-0 depends on its lipid bilayer environment. Exp. Eye Res. 2013; 113:32–40. [PubMed: 23680159]

Truscott RJ. Age-related nuclear cataract: a lens transport problem. Ophthalmic Res. 2000; 32:185–194. [PubMed: 10971179]

Warren GB, Houslay MD, Metcalfe JC, Birdsall NJ. Cholesterol is excluded from the phospholipid annulus surrounding an active calcium transport protein. Nature. 1975; 255:684–687. [PubMed: 124402]

White TW, Bruzzone R. Intercellular communication in the eye: clarifying the need for connexin diversity. Brain Res. Brain Res. Rev. 2000; 32:130–137. [PubMed: 10751662]

White TW, Goodenough DA, Paul DL. Targeted ablation of connexin50 in mice results in microphthalmia and zonular pulverulent cataracts. The Journal of cell biology. 1998; 143:815–825. [PubMed: 9813099]

Widomska J, Raguz M, Dillon J, Gaillard ER, Subczynski WK. Physical properties of the lipid bilayer membrane made of calf lens lipids: EPR spin labeling studies. Biochim. Biophys. Acta. 2007a; 1768:1454–1465. [PubMed: 17451639]

Widomska J, Raguz M, Subczynski WK. Oxygen permeability of the lipid bilayer membrane made of calf lens lipids. Biochim. Biophys. Acta. 2007b; 1768:2635–2645. [PubMed: 17662231]

Wride MA. Lens fibre cell differentiation and organelle loss: many paths lead to clarity. Philosophical transactions of the Royal Society of London. Series B, Biological sciences. 2011; 366:1219–1233.

Yappert MC, Borchman D. Sphingolipids in human lens membranes: an update on their composition and possible biological implications. Chem. Phys. Lipids. 2004; 129:1–20. [PubMed: 14998723]

Yappert MC, Rujoi M, Borchman D, Vorobyov I, Estrada R. Glycero- versus sphingo-phospholipids: correlations with human and non-human mammalian lens growth. Exp. Eye Res. 2003; 76:725–734. [PubMed: 12742355]

Yin JJ, Subczynski WK. Effects of lutein and cholesterol on alkyl chain bending in lipid bilayers: a pulse electron spin resonance spin labeling study. Biophys. J. 1996; 71:832–839. [PubMed: 8842221]

Zampighi GA, Eskandari S, Hall JE, Zampighi L, Kreman M. Micro-domains of AQP0 in lens equatorial fibers. Exp. Eye Res. 2002; 75:505–519. [PubMed: 12457863]

Zelenka PS. Phospholipid composition and metabolism in the embryonic chicken lens. Exp. Eye Res. 1978; 26:267–274. [PubMed: 639879]

Zelenka PS. Lens lipids. Curr. Eye Res. 1984; 3:1337–1359. [PubMed: 6391828]

Zhang Z, Zeng J, Yin H, Tang D, Borchman D, Paterson CA. Membrane lipid alpha-crystallin interaction and membrane Ca2+ -ATPase activities. Curr. Eye Res. 1999; 18:56–61. [PubMed: 10075203]

- Organization of lipids in fiber cell plasma membranes from human lenses was studied.
- Relative amounts of phospholipids and cholesterol in membrane domains were evaluated.
- The relationship between the organization of lipids and proteins is discussed.

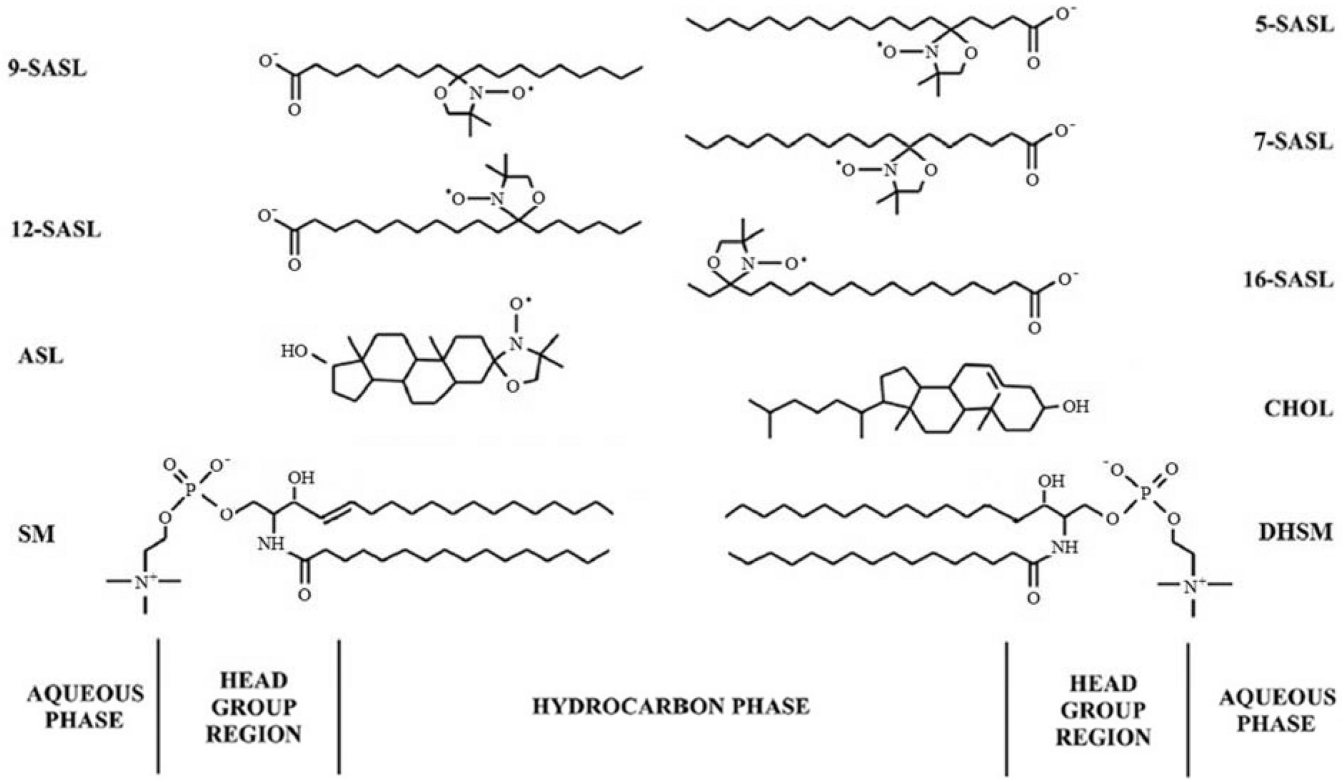

Fig. 1.

Chemical structures of stearic acid- (*n*-SASLs) and Chol-analog spin labels (ASL) together with the structure of Chol (CHOL), palmitoyl sphingomyelin (SM), and palmitoyl dihydrosphingomyelin (DHSM) (the most abundant lipids in human lens membranes). Approximate locations of these molecules across the lipid bilayer membrane are illustrated.

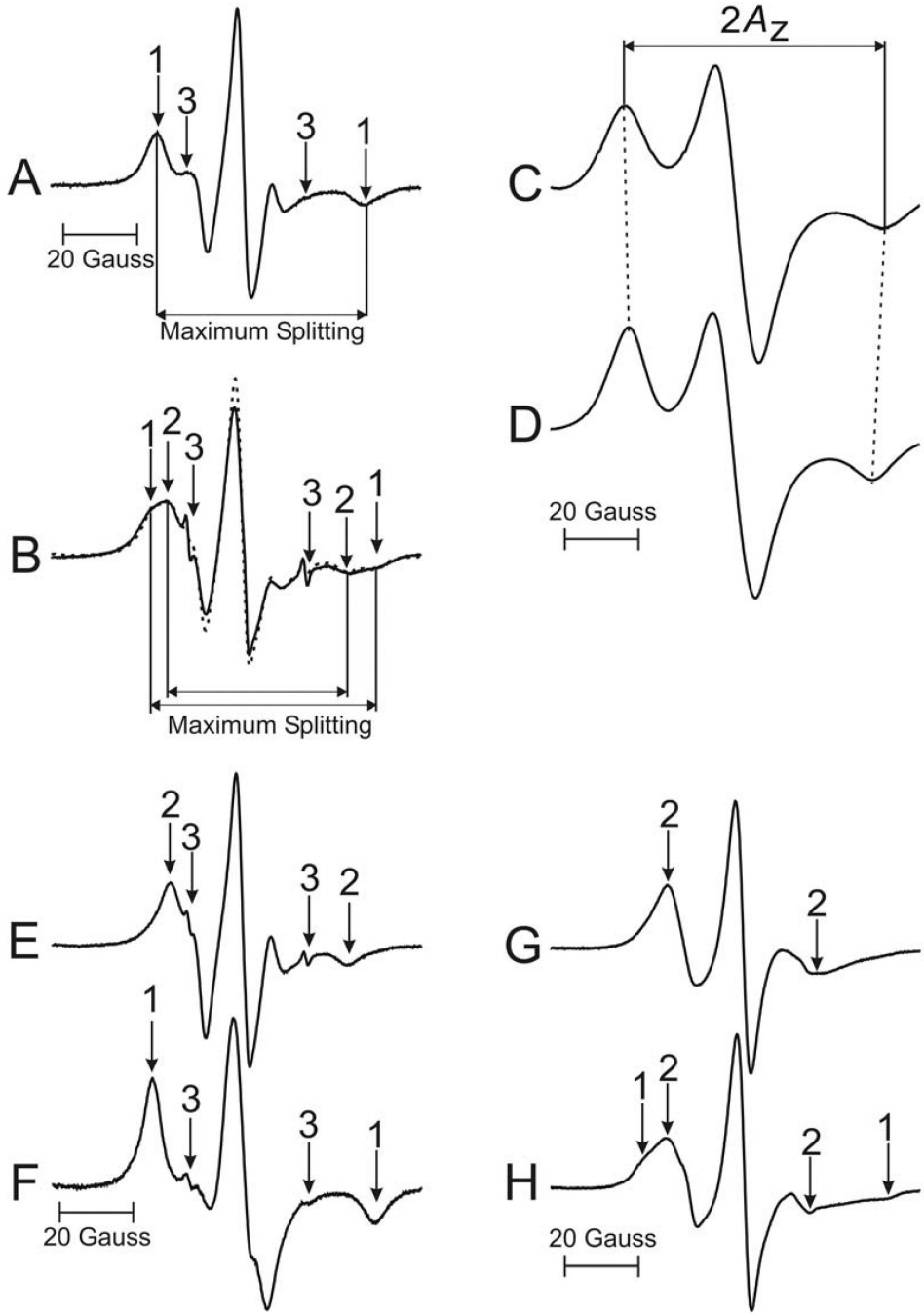

Fig. 2.

Representative EPR spectra of 5-SASL (A, C) and 12-SASL (B, D) from cortical intact membranes. Spectra (A) and (B) were recorded at 37°C. The measured values used to evaluate maximum splitting are indicated. Spectra (C) and (D) were recorded at −165°C to cancel motional effects. The measured $2A_Z$ value is indicated. EPR spectra of ASL from cortical (G) and nuclear (H) intact membranes, recorded at 37°C. The positions of certain peaks were evaluated with a high level of precision by monitoring them at 10 times higher receiver gain and, when necessary, a higher modulation amplitude. In this figure arrows 1–3 represent spectra from strongly immobilized, weakly immobilized, and water components,

respectively. The procedure for the evaluation of the relative amount of PLs in the bulk domain is illustrated (spectra B, E, F). The experimental EPR spectrum of 12-SASL in the cortical intact membranes (B, solid line) can be simulated (B, dotted line) by adding 63% of spectrum (E) and 37% of spectrum (F). Here (E) is the EPR spectrum of 12-SASL in cortical lens lipid membranes obtained at 37°C and (F) is the EPR spectrum of 12-SASL in cortical lens lipid membranes obtained at −10 °C (this spectrum has the same maximum splitting as the strongly immobilized component in spectrum (B)).

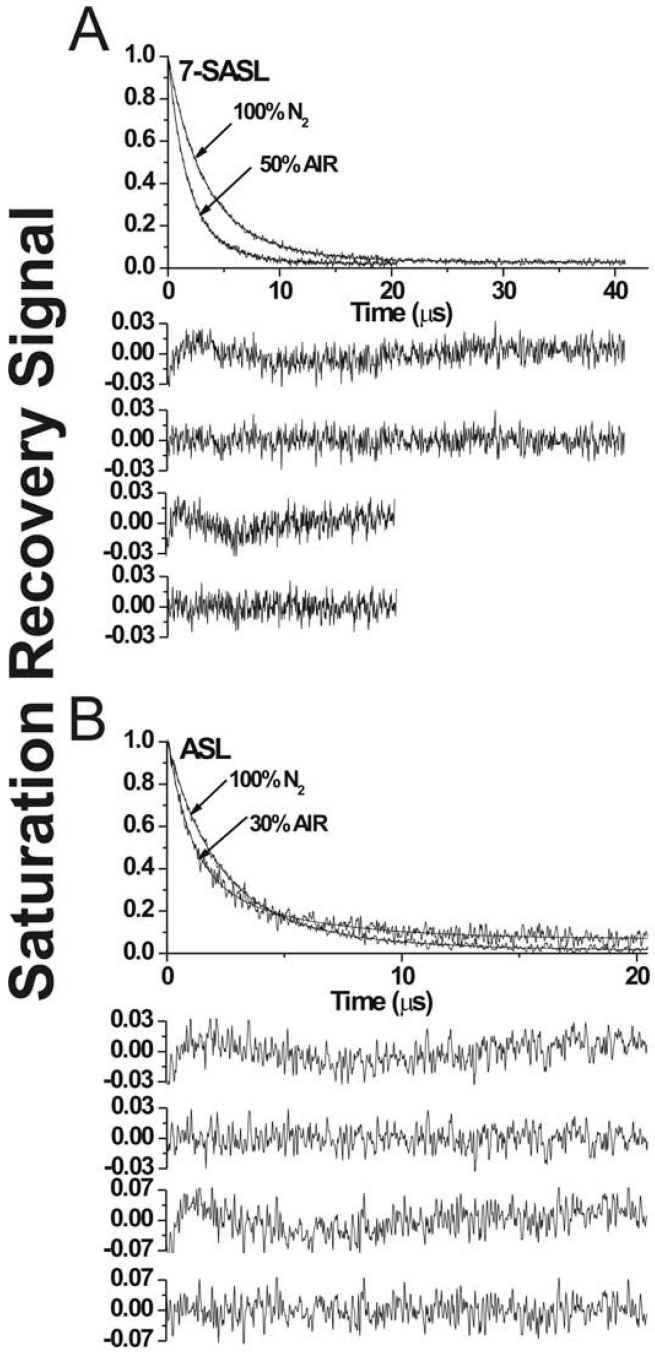

Fig. 3.

Representative SR signals with fitted curves and residuals (the experimental signal minus the fitted curve) for 7-SASL (A) and ASL (B) from cortical intact membranes. Signals were recorded at 37°C for deoxygenated samples (equilibrated with 100% nitrogen) and equilibrated at 37°C with an air/nitrogen gas mixture. For deoxygenated samples the SR signals can be satisfactorily fitted with only a double-exponential function: for 7-SASL, with time constants of 6.18 ± 0.43 μs and 2.82 ± 0.11 μs, and for ASL, with time constants of 4.80 ± 0.39 μs and 1.89 ± 0.07 μs. The first residual is for single- and the second residual for double-exponential fits. The SR signal in the presence of molecular oxygen can be fitted satisfactorily only with a double-exponential function: for 7-SASL, with time constants of

3.11 ± 0.17 μs and 1.44 ± 0.06 μs, and for ASL, with time constants of 4.47 ± 0.31 μs and 0.98 ± 0.05 μs. The third residual is for single- and the fourth residual for double-exponential fits.

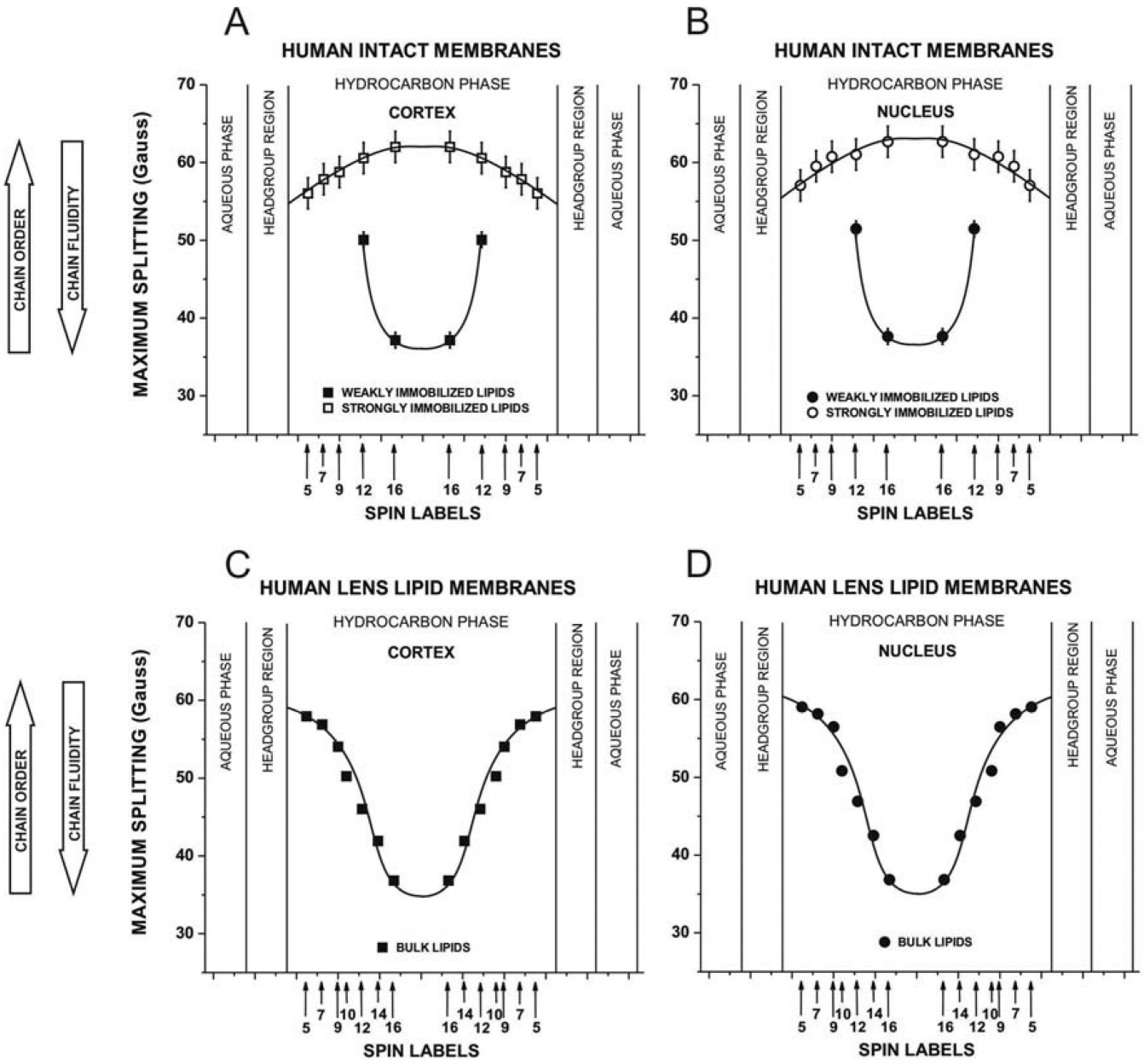

Fig. 4.

Profiles of the maximum splitting obtained with *n*-SASLs at 37°C for (A) cortical intact membranes and (B) nuclear intact membranes. Profiles are reported for bulk lipids and for boundary plus trapped lipids. For comparison, profiles of the maximum splitting for (C) cortical lens lipid membranes and (D) nuclear lens lipid membrane are included. Values for lens lipid membranes were taken from measurements reported in Mainali et al., 2013b, where different displays, namely profiles of the order parameter, were presented. Maximum splitting (mean values and standard deviations) obtained with 12-SASL from three different preparations of membranes from eyes of three different donors are 58.81 G ± 2.0 G for bulk lipids and 51.58 G ±1.33 G for boundary plus trapped lipids in cortex and 60.05 G ±2.68 G for bulk lipids and 51.61 G ±1.51 G for boundary plus trapped lipids in nucleus. Approximate localizations of the nitroxide moieties of spin labels are indicated by arrows.

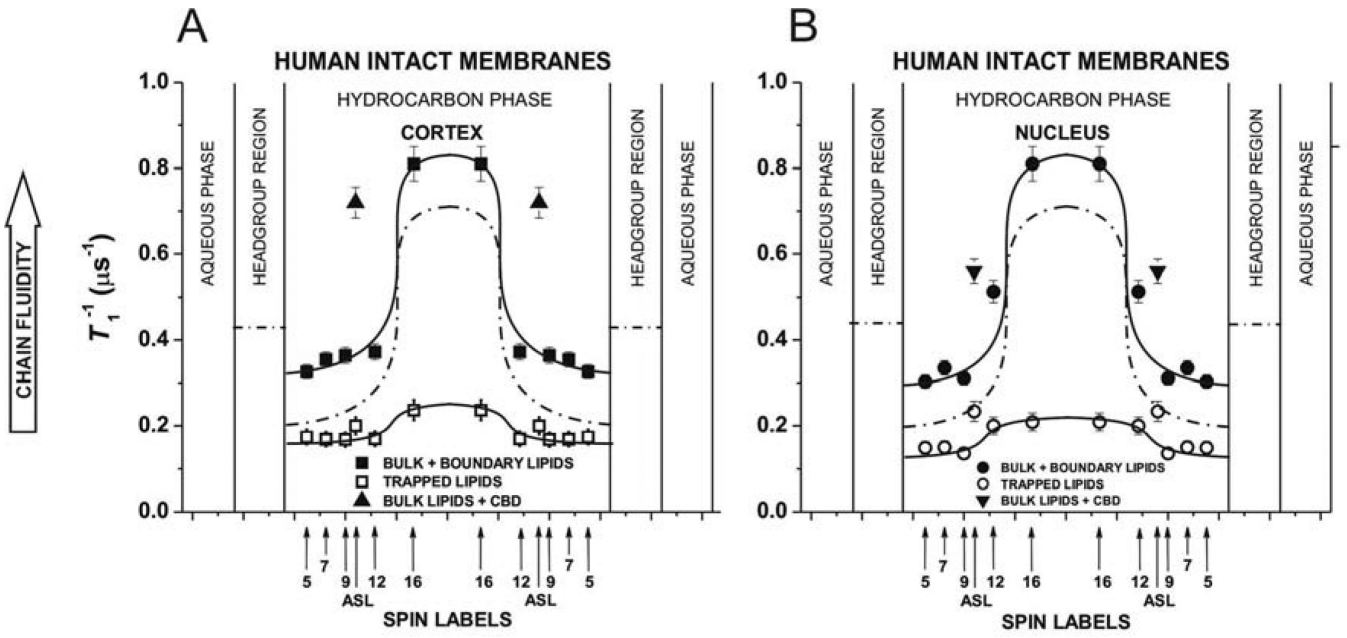

Fig. 5.

Profiles of T_1^{-1} (the spin-lattice relaxation rate) obtained with *n*-SASLs at 37°C for (A) cortical and (B) nuclear intact membranes. Profiles are reported for bulk plus boundary lipids and for trapped lipids. T_1^{-1} (mean values and standard deviations) obtained with 12-SASL from three different preparations of membranes from eyes of three different donors are 0.56 ±0.34 μs^{-1} for bulk plus boundary lipids and 0.20 ±0.03 μs^{-1} for trapped lipids in cortex and are 0.64 ±0.24 μs^{-1} for bulk plus boundary lipids and 0.21 ±0.02 μs^{-1} for trapped lipids in nucleus. Values of T_1^{-1} obtained with ASL in domains of cortical and nuclear membranes are also included. Superimposed are profiles for cortical (A) and nuclear (B) lens lipid membranes (broken lines drawn based on data presented in (Mainali et al., 2013b)). Approximate localizations of the nitroxide moieties of spin labels are indicated by arrows.

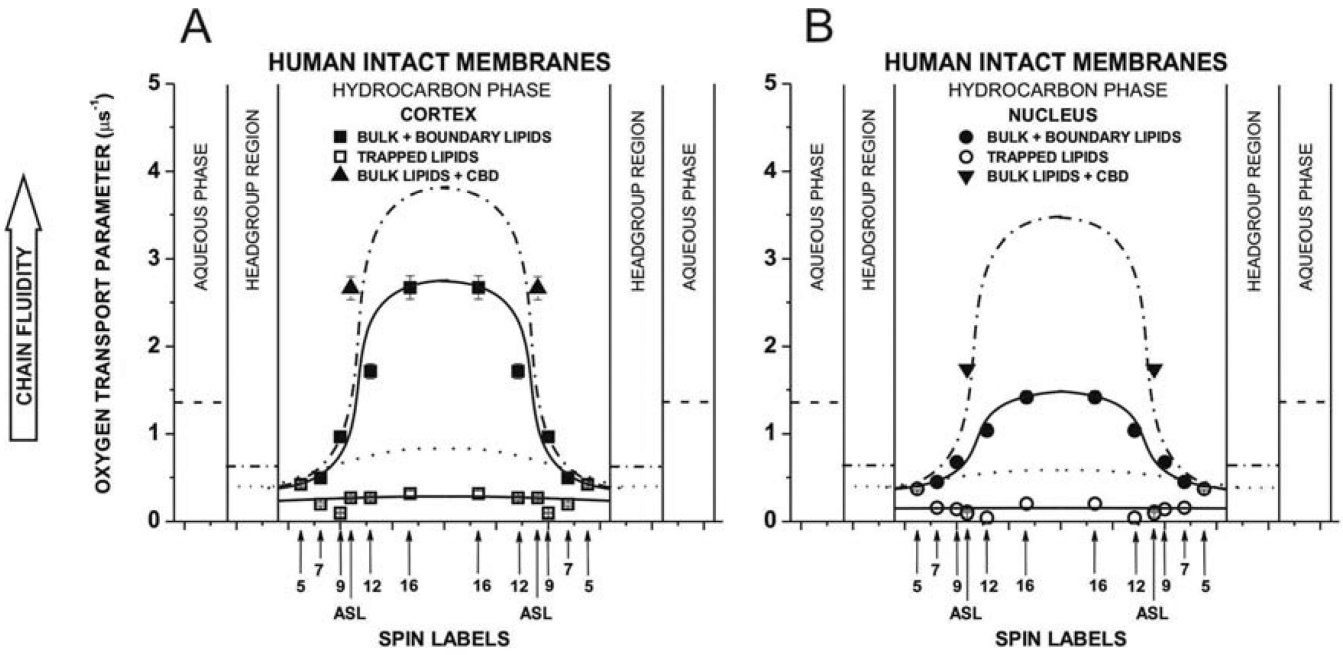

Fig. 6.

Profiles of the OTP obtained with *n*-SASLs at 37°C for (A) cortical and (B) nuclear intact membranes. Profiles are reported for bulk plus boundary lipids and for trapped lipids. OTP (mean values and standard deviations) obtained with 12-SASL from three different preparations of membranes from eyes of three different donors are 1.84 ±0.65 μs^{-1} for bulk plus boundary lipids and 0.31 ±0.12 μs^{-1} for trapped lipids in cortex and are 1.61 ±0.60 μs^{-1} for bulk plus boundary lipids and 0.22 ±0.12 μs^{-1} for trapped lipids in nucleus. Values obtained with ASL in domains of cortical and nuclear membranes are also included. Superimposed are profiles for cortical (A) and nuclear (B) lens lipid membranes (broken (bulk domain) and dotted (CBD) lines drawn based on data presented in (Mainali et al., 2013b)). Approximate localizations of the nitroxide moieties of spin labels are indicated by arrows.

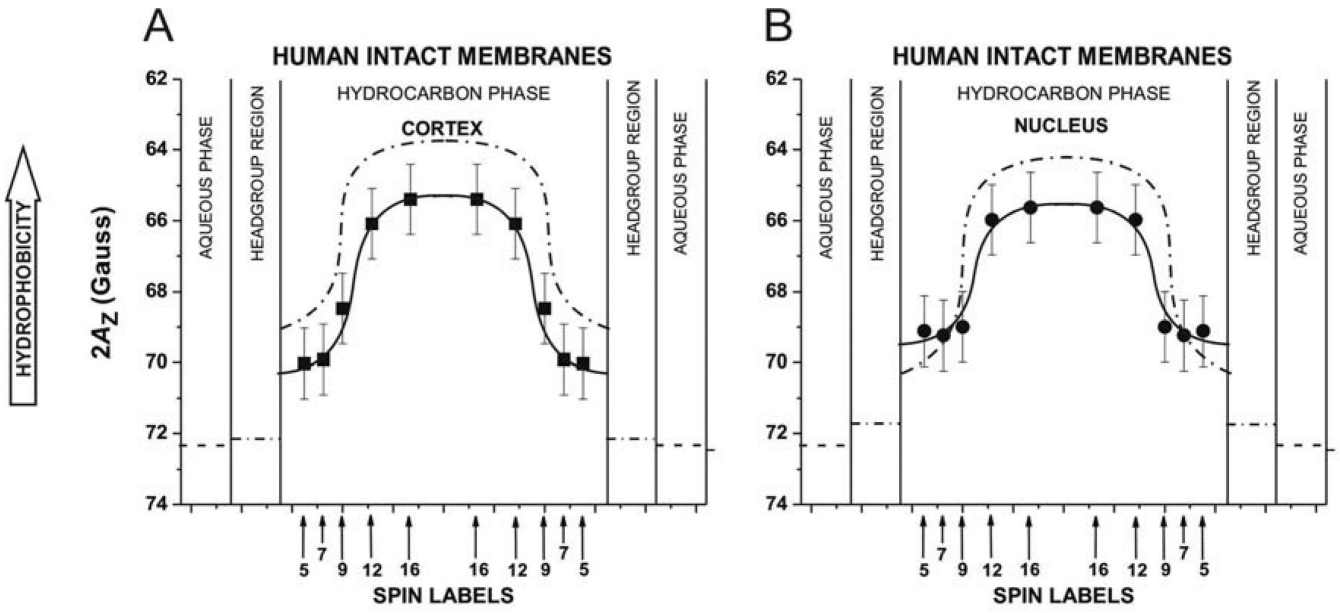

Fig. 7.

Profiles of hydrophobicity ($2A_Z$) obtained with *n*-SASLs for (A) cortical and (B) nuclear intact membranes. Profiles represent averaged values from bulk, boundary, and trapped lipids. $2A_Z$ (mean values and standard deviations) obtained with 12-SASL from three different preparations of membranes from eyes of three different donors are 65.24 ±0.73 G for cortical membranes and are 65 ±0.80 G for nuclear membranes. Superimposed are profiles for cortical (A) and nuclear (B) lens lipid membranes (broken lines drawn based on data presented in (Mainali et al., 2013b)). Approximate localizations of the nitroxide moieties of spin labels are indicated by arrows.

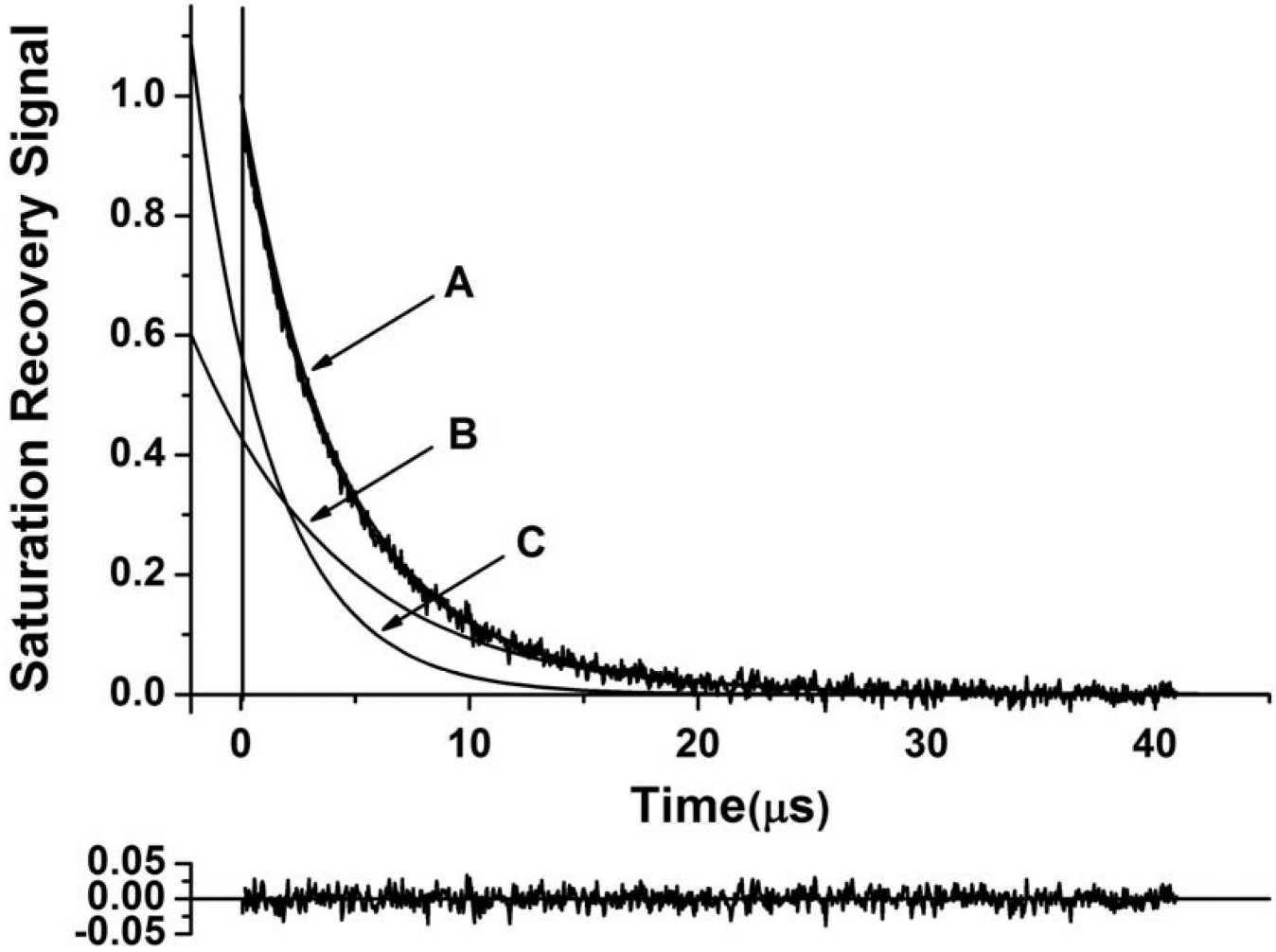

Fig. 8.

The illustration of the procedure for the evaluation of the relative amount of PLs in the trapped domain. The SR EPR signal of 12-SASL in the deoxygenated cortical intact membrane obtained at 37°C (A). This signal can be successfully fitted with only a double-exponential function with time constants of 6.1 ± 0.20 μs (B) and 2.53 ± 0.04 μs (C). The residual (the experimental signal minus fitted curves), shown in the bottom, indicates the goodness of the fit. The contribution of each component to the experimental signal is given by the pre-exponential coefficients obtained from the fitting program. Because the SR signal is recorded with the delay (in our case 2.2 μs) after the end of the saturating pulse, we have to extrapolate back the exponentials for (B) and (C) components to get actual ratio of their pre-exponential coefficients.

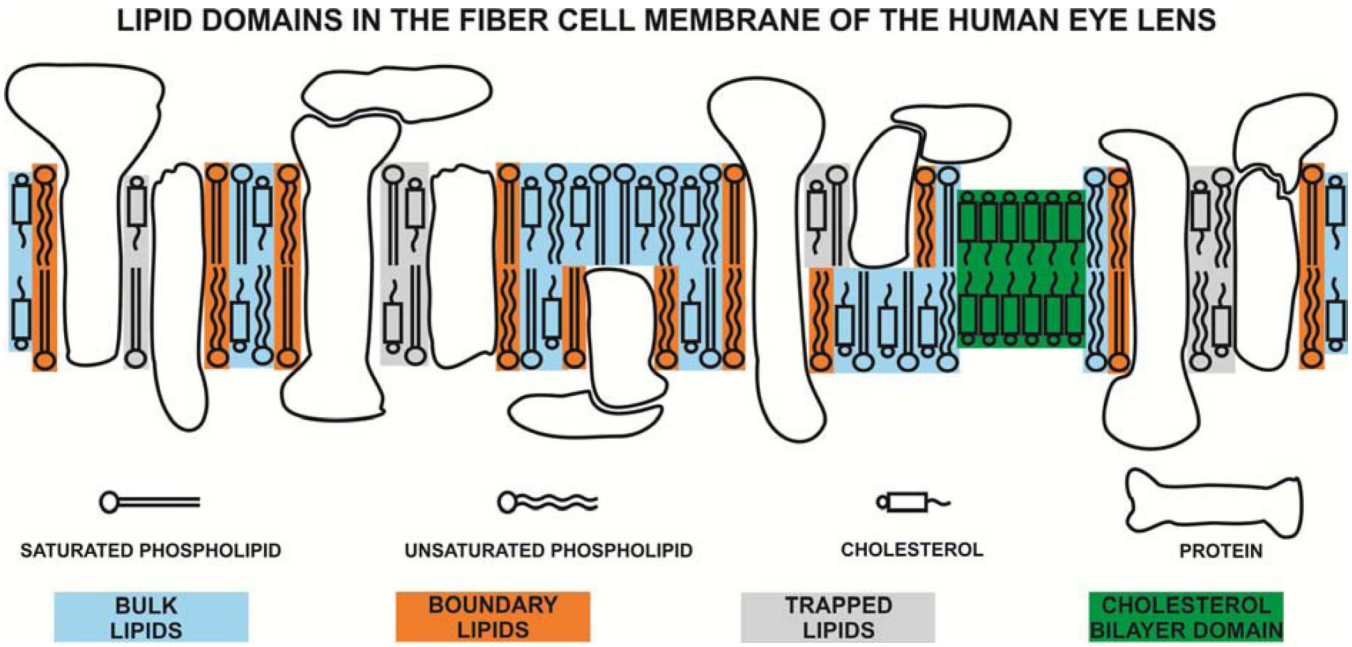

Fig. 9.

Schematic drawing of the lens intact membrane. Purported lipid domains induced by the high Chol content and the presence of integral membrane proteins are indicated. Note that Chol is excluded from boundary lipids.

Table 1

Permeability coefficients for oxygen (P_M) across the hydrocarbon region of domains in human intact and lens lipid membranes at 37 °C

	P_M(cm/s)
Cortical intact membranes (bulk + boundary lipids)	66.3 ±20
Nuclear intact membranes (bulk + boundary lipids)	53.8 ±16
Cortical intact membranes (trapped lipids)	16.8 ±5.0
Nuclear intact membranes (trapped lipids)	8.5 ±2.5
Water layer[a]	94.4 ±28
Cortical lens lipid membranes (bulk lipids)[b]	76.5 ±23
Nuclear lens lipid membranes (bulk lipids)[b]	71.2 ±21
Cortical lens lipid membranes (CBD)[c]	40 ±12
Nuclear lens lipid membranes (CBD)[c]	32 ±9.6
Water layer of the same thickness as the CBD[c]	89 ±27

[a] The thickness of the water layer is the same as the hydrocarbon region.

[b] P_M was calculated based on oxygen transport parameter profiles presented in Mainali et al., 2013c.

[c] Data taken from Mainali et al., 2013c.

Table 2

Distribution of PLs (% of total PLs) between domains in human intact lens membranes

Conventional EPR (12-SASL)	Bulk Lipids	Boundary + Trapped Lipids
Cortex	63 ±5 (65.5 ±5.5)[a]	37 ±5 (34.5 ±5.5)[a]
Nucleus	54 ±5 (51.5 ±6.5)[a]	46 ±5 (48.5 ±6.5)[a]
SR EPR (12-SASL)	Bulk + Boundary Lipids	Trapped Lipids
Cortex	64 ±6.4 (48 ±20)[a]	36 ±1.8 (52 ±20)[a]
Nucleus	49 ±4.9 (29 ±17)[a]	51 ±2.6 (71 ±17)[a]

[a]Data (mean values and standard deviations) obtained for three different preparations of cortical and nuclear membranes from eyes of three different donors. Averages were significantly different with *P* values determined by Student's *t*-test: $P = 0.018$ for conventional EPR data and $P = 0.274$ for SR EPR data.

Student's *t*-test results for. Limited amounts of samples and low signal-to-noise ratio strongly affected accuracy of SR EPR measurements

Table 3

Distribution of Chol (% of total Chol) between domains in human intact lens membranes

Conventional EPR (ASL)	Bulk Lipids + CBD[a]	Trapped Lipids
Cortex	100 ±5	0 ±5
Nucleus	50 ±5	50 ±5
SR EPR (ASL)	Bulk Lipids + CBD[a]	Trapped Lipids
Cortex	77 ±7.7	23 ±1.2
Nucleus	54 ±5.4	46 ±2.3

[a]Chol and ASL is substantially excluded from boundary lipid domain